NAVAL POSTGRADUATE SCHOOL

MONTEREY, CALIFORNIA

THESIS

APPLICATION OF THE COMMUNITY RADIATIVE TRANSFER MODEL TO EVALUATE SATELLITE-BASED MEASUREMENTS ACROSS THE AFRICAN EASTERLY JET OVER WESTERN AFRICA

by

Richard D. Ernest

March 2007

Thesis Co-Advisors: Nancy Baker
                                 Russell L. Elsberry

Approved for public release; distribution is unlimited

THIS PAGE INTENTIONALLY LEFT BLANK

REPORT DOCUMENTATION PAGE		*Form Approved OMB No. 0704-0188*

Public reporting burden for this collection of information is estimated to average 1 hour per response, including the time for reviewing instruction, searching existing data sources, gathering and maintaining the data needed, and completing and reviewing the collection of information. Send comments regarding this burden estimate or any other aspect of this collection of information, including suggestions for reducing this burden, to Washington headquarters Services, Directorate for Information Operations and Reports, 1215 Jefferson Davis Highway, Suite 1204, Arlington, VA 22202-4302, and to the Office of Management and Budget, Paperwork Reduction Project (0704-0188) Washington DC 20503.

1. AGENCY USE ONLY *(Leave blank)*	2. REPORT DATE March 2007	3. REPORT TYPE AND DATES COVERED Master's Thesis	
4. TITLE AND SUBTITLE Application of the Community Radiative Transfer Model to Evaluate Satellite-Based Measurements Across the African Easterly Jet over Western Africa		5. FUNDING NUMBERS	
6. AUTHOR(S) Richard D. Ernest			
7. PERFORMING ORGANIZATION NAME(S) AND ADDRESS(ES) Naval Postgraduate School Monterey, CA 93943-5000		8. PERFORMING ORGANIZATION REPORT NUMBER	
9. SPONSORING /MONITORING AGENCY NAME(S) AND ADDRESS(ES) N/A		10. SPONSORING/MONITORING AGENCY REPORT NUMBER	
11. SUPPLEMENTARY NOTES The views expressed in this thesis are those of the author and do not reflect the official policy or position of the Department of Defense or the U.S. Government.			
12a. DISTRIBUTION / AVAILABILITY STATEMENT Approved for public release; distribution is unlimited		12b. DISTRIBUTION CODE A	

13. ABSTRACT (maximum 200 words)

   The Community Radiative Transfer Model (CRTM) has been used to determine which polar-orbiter satellite channels are best suited to remotely sense in a cloud-free environment the lower-tropospheric temperature and moisture gradients that determine the location and intensity of the African Easterly Jet over West Africa. This study evaluates the capability of five microwave sensors and three infrared sensors, including both conical- and cross-track scanning instruments. Atmospheric profiles obtained during the JET2000 field experiment blended with the European Center for Medium-range Weather Forecasting model analyses are input in the CRTM to obtain brightness temperature outputs. To address separately the moisture (temperature) signature, the average of the northern and southern temperature (moisture) profiles were combined with the real moisture (temperature) profiles. The effects of land surface emissivity uncertainty of +/-3% for microwave and +/-1% for infrared were tested. From the total set of 423 channels evaluated, 11 microwave and 21 infrared channels were found appropriate for obtaining moisture gradient information, but after applying emissivity perturbations this list was reduced to two microwave and 20 infrared channels. Temperature gradient information was determined to be available from 35 microwave channels and 95 infrared channels, with no impacts noted due to emissivity perturbations.

14. SUBJECT TERMS Microwave satellite, Infrared satellite, Polar-orbiter, Community Radiative Transfer Model, African Easterly Jet, JET2000			15. NUMBER OF PAGES 91
			16. PRICE CODE
17. SECURITY CLASSIFICATION OF REPORT Unclassified	18. SECURITY CLASSIFICATION OF THIS PAGE Unclassified	19. SECURITY CLASSIFICATION OF ABSTRACT Unclassified	20. LIMITATION OF ABSTRACT UL

NSN 7540-01-280-5500

Standard Form 298 (Rev. 2-89)
Prescribed by ANSI Std. 239-18

THIS PAGE INTENTIONALLY LEFT BLANK

APPLICATION OF THE COMMUNITY RADIATIVE TRANSFER MODEL TO EVALUATE SATELLITE-BASED MEASUREMENTS ACROSS THE AFRICAN EASTERLY JET OVER WESTERN AFRICA

Richard D. Ernest
Captain, United States Air Force
B.S., University of South Alabama, 2001

Submitted in partial fulfillment of the
requirements for the degree of

MASTER OF SCIENCE IN METEOROLOGY

from the

**NAVAL POSTGRADUATE SCHOOL
March 2007**

Author: Richard D. Ernest

Approved by: Nancy Baker
                 Thesis Co-Advisor

                 Russell L. Elsberry
                 Thesis Co-Advisor

                 Phillip A. Durkee
                 Chairman, Department of Meteorology

iii

THIS PAGE INTENTIONALLY LEFT BLANK

ABSTRACT

The Community Radiative Transfer Model (CRTM) has been used to determine which polar-orbiter satellite channels are best suited to remotely sense in a cloud-free environment the lower-tropospheric temperature and moisture gradients that determine the location and intensity of the African Easterly Jet over West Africa. This study evaluates the capability of five microwave sensors and three infrared sensors, including both conical- and cross-track scanning instruments. Atmospheric profiles obtained during the JET2000 field experiment blended with the European Center for Medium-range Weather Forecasting model analyses are input in the CRTM to obtain brightness temperature outputs. To address separately the moisture (temperature) signature, the average of the northern and southern temperature (moisture) profiles were combined with the real moisture (temperature) profiles. The effects of land surface emissivity uncertainty of +/-3% for microwave and +/-1% for infrared were tested. From the total set of 423 channels evaluated, 11 microwave and 21 infrared channels were found appropriate for obtaining moisture gradient information, but after applying emissivity perturbations this list was reduced to two microwave and 20 infrared channels. Temperature gradient information was determined to be available from 35 microwave channels and 95 infrared channels, with no impacts noted due to emissivity perturbations.

THIS PAGE INTENTIONALLY LEFT BLANK

TABLE OF CONTENTS

LIST OF FIGURES

THIS PAGE INTENTIONALLY LEFT BLANK

LIST OF TABLES

THIS PAGE INTENTIONALLY LEFT BLANK

ACKNOWLEDGMENTS

THIS PAGE INTENTIONALLY LEFT BLANK

I. INTRODUCTION

A. MOTIVATION

Tropical weather forecasting is a challenging and important venture. Intensity forecasts for tropical cyclones (TC) in the eastern Atlantic Ocean have significant impacts on what type of response actions will be taken by those within the path of these destructive weather events. Many of these Atlantic storms evolve from disturbances that evolve over western North Africa as African Easterly Waves (AEW). The AEW's develop in association with the African Easterly Jet (AEJ), which exists between the hot, dry air over the Sahara Desert to the north and warm, moist air to the south. However, recent research (Karyampudi and Pierce 2002; Thorncroft et al. 2003; Dunion and Velden 2004) suggests the formation and intensification of Atlantic tropical cyclones may depend on the presence of the Saharan Air Layer (SAL). This dusty air mass originates over the arid Sahara Desert, and eventually propagates eastward off the West African coast.

The effects of the SAL on TC activity have been hypothesized to have both negative and positive impacts on tropical cyclones depending on the relative location of the TC to the SAL. Karyampudi and Pierce (2002) examined the effect of the SAL on tropical cyclone seedlings. They found that a weaker SAL and a narrow AEJ provided positive contributions to the subsequent development of Tropical Storm Luis and Hurricane Ernesto. Negative impacts of the SAL were found in the case of Hurricane Andrew, which developed into a devastating hurricane after escaping the effects of the SAL near the east Florida coast. The negative impact of the SAL on TC activity was further examined by Dunion and Velden (2004) in which three factors were identified as being detrimental to TC development: increased vertical wind shear from the AEJ; dry air entrainment from the SAL; and an enhancement of the trade wind inversion that defines the lower boundary of the SAL.

1

Unfortunately, the source region in which the SAL originates is one of the most data-sparse regions of the world. Limited in-situ weather observations are available, but they are not dense enough in space and time to resolve the complex weather conditions over this critical region. One of the best in-situ datasets measuring the AEJ over this area came from the JET2000 experiment conducted from 25-30 August 2000. Recent work conducted during the 2006 African Multidisciplinary Monsoon Activity (AMMA) also concentrated on observing the interconnected features of the SAL, AEWs, and the AEJ.

Military operations in this region are very likely in the future due to the persistent political unrest of the West African region, which is attractive to terrorist organizations looking to operate freely in these remote regions (Whelan 2005). In response, the Department of Defense (DoD) is currently planning to create a new unified command in Africa (Air Force News 2006). With an increase in military assets operating in support of this new command, and the potential for severe weather in the vast regions of ungoverned space, a complete understanding of the weather phenomena over the Sahel is necessary.

B. BACKGROUND

1. The African Easterly Jet

The presence of the AEJ over western Africa is a significant feature in the development of tropical phenomena, since it can provide energy to AEWs under the right circumstances. The AEJ forms due to a baroclinic zone that arises from the meridional thermal contrast between the cooler, moist air to the south and the hot, dry air of the SAL. A conceptual model of the AEJ is illustrated in Figure 1. While the AEJ originates over land, it continues to exist off the West African coast, since radiative heating of dust contained within in the SAL contributes to the maintenance of the baroclinity necessary for the jet to exist (Karyampudi and Carlson 1988). This AEJ extension provides some of the energy needed to support wave amplification over the eastern Atlantic. The presence of the AEJ provides cyclonic shear vorticity to the south of the AEJ maximum, as well as a corresponding area of anticyclonic shear vorticity to the north of the jet. The maximum amount of shear is found at the maximum level of the AEJ winds—

typically around 650 mb. Burpee (1972) found that the impact of horizontal and vertical shear to the south of the AEJ satisfied the criteria for barotropic-baroclinic instability as proposed by Charney and Stern (1962).   Westward-propagating AEWs south of the AEJ can gain energy from the AEJ through conversion of zonal kinetic energy into eddy kinetic energy.
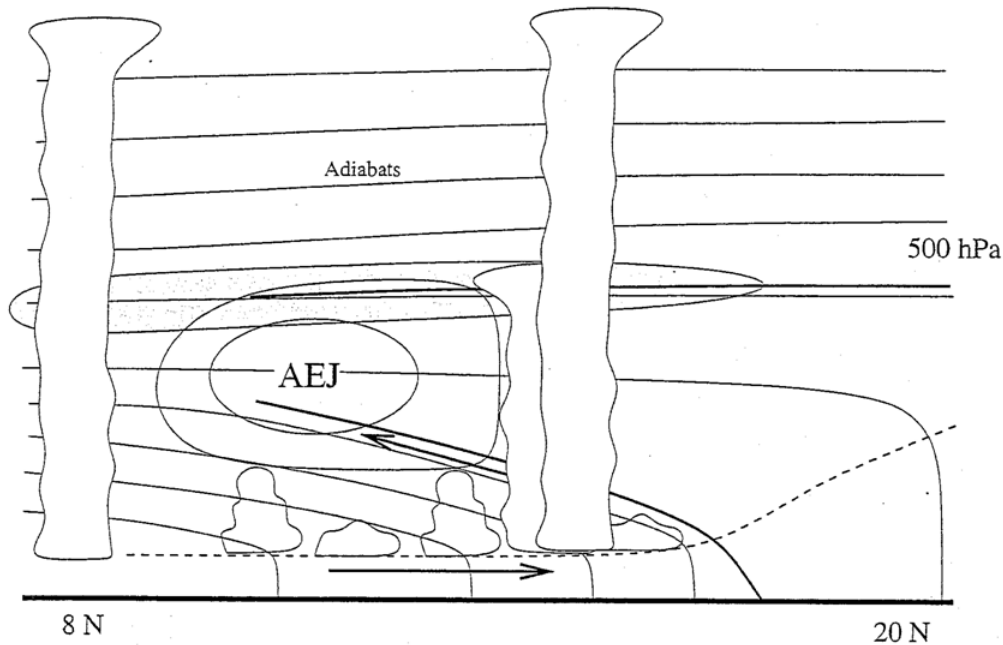
Figure 1.   Conceptual model of the thermally direct circulation resulting in the AEJ. Mixed layer top denoted by dashed line, solid line denote adiabats. Within the southern air mass to the south of the AEJ, deep moist convection dominates. To the north, intermittent dry convection exists (Parker et al. 2006).

The location of the AEJ can vary significantly between dry and wet Sahelian years (Thorncroft et al. 2003). During dry years, the AEJ is typically displaced toward the equator due to the larger horizontal extent of the SAL. During the JET2000 experiment, the AEJ was approximately 5 degrees latitude equatorward of its expected location during a period of relatively dry Sahelian conditions. Accurately depicting the location of the AEJ in numerical weather prediction (NWP) models may be a key component as to whether the SAL may have a positive or negative influence on the formation and intensification of a tropical cyclone seedling in subsequent NWP forecasts.

3

The majority of the hurricanes that form in the Atlantic basin begin as an AEW that originates over Africa. More importantly, as many as 85% of the most intense storms (Saffir-Simpson category three and higher) have been found to originate from AEWs (Landsea 1993). The AEW has a period of about 3-5 days, a wavelength of 2000-4000 km, and a westward propagation speed of approximately 7-9 ms^{-1} (Reed et al. 1977). The structure of the AEW is complex, and may be multi-centered with a southern vorticity maximum at the 650 mb level to the south of the AEJ, and a corresponding northern vorticity center at approximately 850 mb to the north of the AEJ (Pytharoulis and Thorncroft 1999).

2. The Saharan Air Layer

The SAL is an elevated layer of very dry, hot, and dusty air that overrides much cooler, moist marine air flowing eastward across the western African continent under the influence of low-level equatorial westerly flow. These equatorial westerlies in the near-surface environment are a response to the intense surface heating experienced over the Sahara desert during summer months. This continental heating leads to the development of thermal lows over the desert. In combination with northeasterly flow to the north of the thermal low, a continental monsoon trough is created over western Africa.

The low-level air mass over West Africa is characterized as being relatively cool and moist compared to the overrunning hot and dry air of the SAL. Once the SAL leaves the African coast, the easterly flow advects it westward over the Atlantic as far as the Caribbean (Carlson and Prospero 1972). The base of the SAL rises to a maximum height of approximately 2.0 to 2.5 km over the Caribbean (Karyampudi and Carlson 1988). Recent satellite measurements (Dunion and Velden 2004) have shown that the wavelength of the SAL may be

as large as 4000-5000 km. A conceptual image of the SAL over western Africa is shown in Figure 2. The southern boundary of the SAL is typically delineated by the AEJ.

Burpee (1972) and Karyampudi and Pierce (2002) have shown that the AEJ can have a positive influence on AEW intensification, but the dry, dusty nature of the SAL to the north of the AEJ has been shown by Dunion and Velden to be a negative factor in TC development. The nature of the contribution to intensification is dependent on the location of the wave in relation to the AEJ, which is controlled by the lower-tropospheric temperature and moisture gradients over continental West Africa.
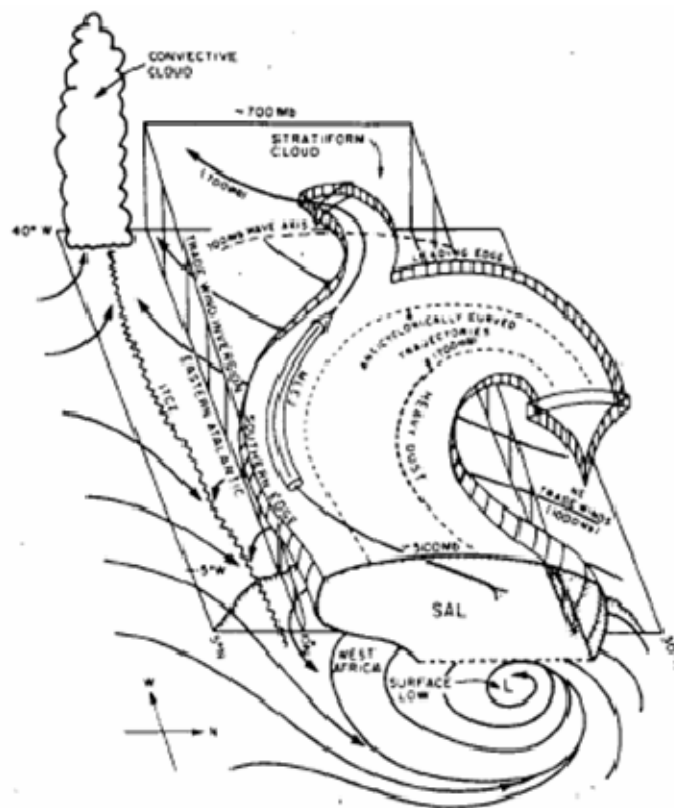
Figure 2.   Three-dimensional model of the SAL looking east to west (Karyampudi and Carlson 1988).

3. Remote Sensing

The assimilation of satellite information in NWP provides large amounts of data in a relatively short amount of time. The challenge for meteorologists is to know how to best use this unique data in support of operational forecasting needs. As of September 2005, the number of observations provided by satellites was on the order of 10^6 daily, although only 10% of this data are currently being used in operational models (LeMarshall et al. 2005). For example, the National Centers for Environmental Prediction (NCEP) indicated that the number of satellite observations received during the month of May 2006 was an astounding 175,533,636, but only 5,017,629 of these observations were assimilated into numerical models. This equates to only a 2.85% usage rate for the available data (NCEP 2006). The problem of using satellite data in the best way is further compounded when one considers that the number of daily satellite observations is expected to increase to the order of 10^{11} by the year 2010 (LeMarshall et al. 2005).

High resolution global satellite data are provided twice daily by polar-orbiting earth satellites (POES) depending on latitude. POES satellite data make up the predominant source for satellite data assimilated into NWP models versus Geostationary Orbiting Earth Satellites (GOES). Two predominant types of POES instruments are used—cross-track scanning and conical-scanning. Cross-track scanning instruments use a sweeping scan motion that results in a variable resolution across the scan width. Resolution differences across the scan width on the Advanced Microwave Sounding Unit A and B (AMSU A/B) and the Microwave Sounding Unit (MSU) are illustrated in Figure 3.
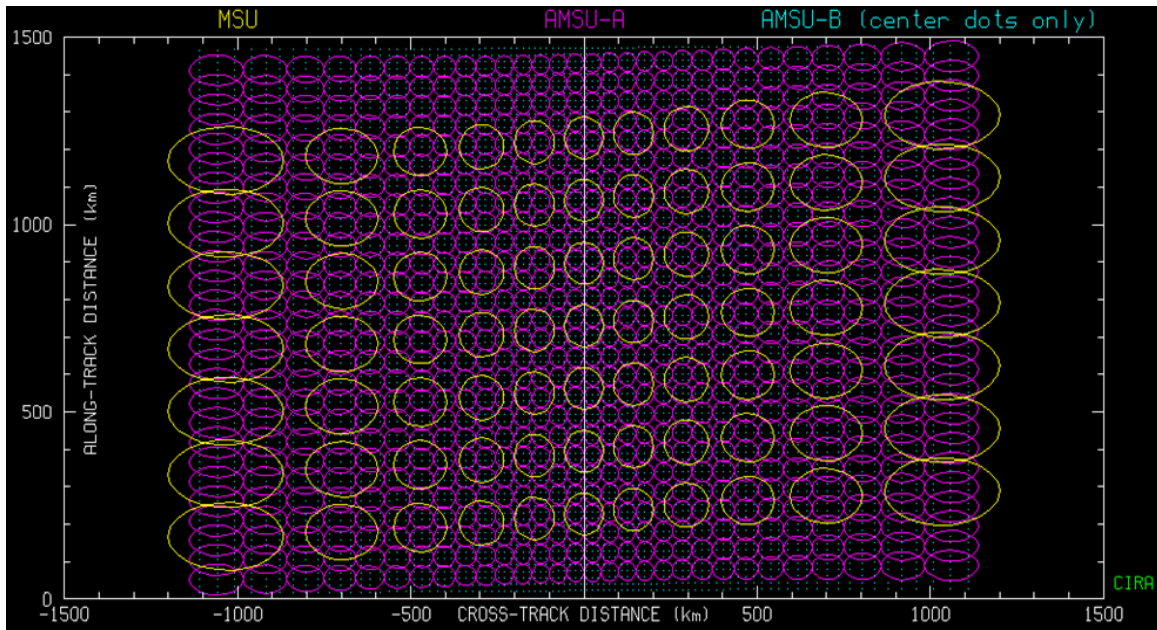
Figure 3. Resolution cells for the AMSU-A (purple circles), AMSU-B (blue dots), and MSU (yellow circles) illustrating the variability in resolution from nadir to the edge of scan [From http://amsu.cira.colostate.edu].

Conical-scanning MW instruments, such as the Advanced Microwave Scanning Radiometer-Earth system (ASMR-E) and the Special Sensing Microwave Imager / Sounder (SSMI/S) have the advantage of providing a constant viewing angle and nearly uniform resolution throughout the scan swath. Conical-scanning instruments also are better suited to separate the horizontal (H) and vertical (V) components of the electromagnetic (EM) radiation received at the satellite sensor. The ability for some channels to separately sense the horizontal and vertical polarizations of received radiation along with the constant viewing angle allows users to derive surface properties less ambiguously than those measured by cross-track scanning MW instruments which mix the polarization signal.

Depending on the application, remote sensing of the atmosphere typically concentrates on those portions of the EM spectrum that are sensitive to particular atmospheric constituents or those regions in which the atmosphere is transparent and information about the Earth surface can be obtained. An indication of the transparency of the atmosphere is given by the atmospheric transmittance, which

7

describes the probability that a photon at a particular wavelength will make it to the top of the atmosphere (TOA). Regions of the EM spectrum that exhibit transmittance values near one are commonly referred to as atmospheric windows. These windows are useful for obtaining remotely-sensed information about the lower troposphere and Earth surface. Figures 4 and 5 illustrate the atmospheric transmittance for the IR and MW spectrums, respectively.
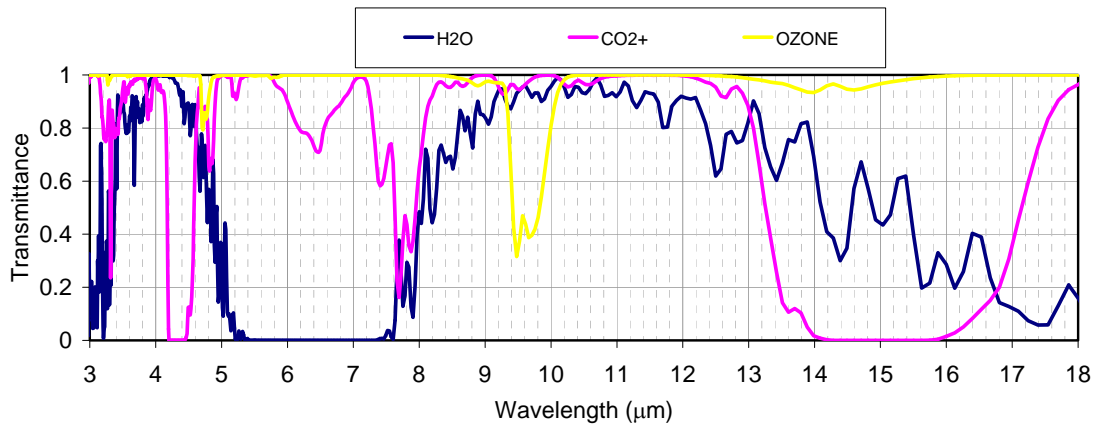
Figure 4. The vertical gaseous atmospheric transmittance of the IR spectrum from 3 to 18 microns. Atmospheric constituents responsible for absorption are listed along the top. Source: Mid-latitude Summer data base of MODTRAN.
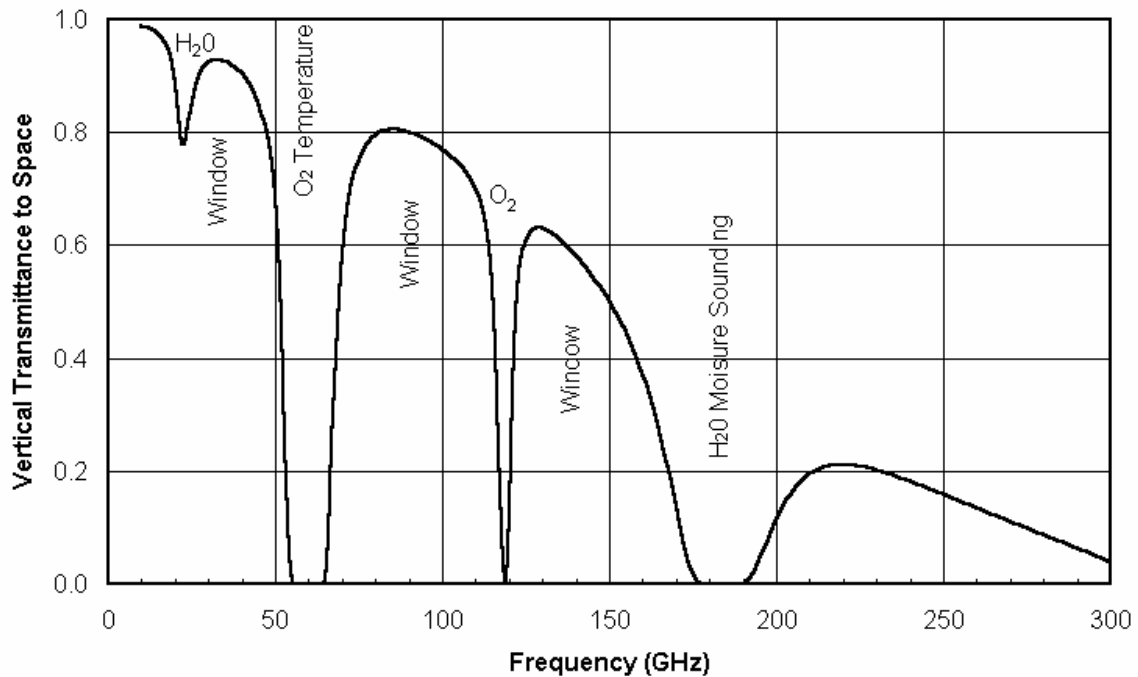
Figure 5.   Vertical atmospheric transmittance of the MW spectrum highlighting water vapor and oxygen as the two main constituents affecting transmission [From http://amsu.cira.colostate.edu].

C.   THESIS OBJECTIVES

Due to the lack of sufficient in-situ observations over the West Africa region, the availability of remotely-sensed data could potentially provide significant information regarding the lower-tropospheric temperature and moisture gradients that control the AEJ. The variability of the AEJ over the Sahel and the eastern Atlantic Ocean has implications on the potential for TC development. The significant increase in the amount of remotely sensed data in recent years has increased the usefulness of satellite data not only as a source for real-time analysis of weather features, but also in the assimilation of this unique data into NWP models.

The objective of this research is to identify the minimum set of polar-orbiting satellite sensor and channels to resolve the lower-tropospheric temperature and moisture gradients that control the location and intensity of the AEJ. An evaluation of eight current sensors is performed to identify which instruments are capable of providing the best satellite information.

9

THIS PAGE INTENTIONALLY LEFT BLANK

II. DATA AND METHODS

A. THE JET2000 EXPERIMENT

The data used in this study were derived from a set of dropsondes deployed during the JET2000 experiment. During the experiment period of 25-30 August 2000, a total of 112 dropsondes were deployed during four flights. Two flights were east-west legs between Sal, Cape Verde Islands and Niamey, Niger, and two were flown out of Niamey in a north-south orientation between $8^{o}N$ -$19^{o}N$ along approximately $2.3^{o}E$. During each of the north-south flights, dropsondes were deployed approximately every half degree of latitude, which provided a detailed set of measurements during the climatological peak of African easterly wave (AEW) and rainfall activity over the region. The dropsondes were deployed from pressure levels ranging between 400 and 500 mb and sampled the vertical temperature, humidity, and wind profiles between the SAL on the north and the non-SAL air to the south of the AEJ. These dropsondes provided a high resolution measurement of the structure associated with the AEJ (Thorncroft et al. 2003). This study will explore the capability of various satellite instruments to identify the differences in the temperature and moisture profiles of the SAL and non-SAL air masses in the lower troposphere observed during the 28 August and 29 August JET2000 flights.

B. THE RADIATIVE TRANSFER MODEL

To transfer the observed atmospheric profiles of temperature and moisture into the brightness temperature domain, the Community Radiative Transfer Model (CRTM) developed by the Joint Center for Satellite Data Assimilation was used. The interface for the CRTM was provided by Drs. Ben Ruston, Clay Blankenship, and Nancy Baker of the Naval Research Laboratory (NRL). The CRTM is a computationally fast-forward and adjoint radiative transfer model that is capable of simulating radiance or brightness temperature observations for a variety of satellite instruments. The CRTM uses a version of the Optical Path Transmittance (OPTRAN) model to compute the gaseous optical depth profile. OPTRAN allows for water vapor and ozone as the only variable gases in the

atmosphere, and treats all other gases as fixed. The CRTM also employs a variety of surface emissivity and reflectivity schemes for the infrared (IR) and microwave (MW) spectra, as well as a complete land surface type database (Yong et al. 2005).

The input atmospheric profiles consist of pressure level (mb), atmospheric temperature (K), and the specific humidity (g/kg). Surface variables of skin temperature were defined by using the lowest data level provided by the atmospheric profiles. Land surface type data were specified in the CRTM using one of the 27 available land surface types recognized by the model. Based on the land surface type, the IR emissivity value was assigned by the CRTM using stored values, with MW emissivity values modeled using the NESDIS Microwave Land Emissivity Model (Weng 2006). Using these variables and a specific set of coefficients for each sensor, the CRTM output variables include: brightness temperature, emissivity, atmospheric transmittance, and Jacobians for atmospheric temperature, moisture, and total emissivity.

C.   SATELLITE SENSORS

A variety of IR and MW sensors and channels were selected for evaluation in this study. Both cross-track scanning and conical-scanning instruments were simulated using the CRTM, and Table 1 summarizes the respective sensors and channels evaluated. These instruments represent the current state of the art capability developed, employed, and controlled by organizations within the United States, and are readily available to DoD customers for use. Different generations of satellite sensor technology have also been selected as a way to explore different capabilities between sensors.

Two conical-scanning instruments were selected for evaluation: the National Aeronautics and Space Administration (NASA)-developed Advanced Microwave Scanning Radiometer for the Earth observing system (AMSR-E) and the Defense Meteorological Satellite Program (DMSP) Special Sensor Microwave Imager/Sounder (SSMI/S). AMSR-E is a 12 channel radiometer designed to measure precipitation, cloud water, water vapor, sea-surface winds, sea-surface temperature, sea ice, snow, and soil moisture. This instrument was

launched onboard the Aqua satellite in 2002. The SSMI/S instrument was placed in orbit aboard the DMSP F-16 satellite in 2003. It was designed to measure atmospheric vertical structure and various bulk atmospheric and surface properties using 12 channels in seven frequencies.

Table 1.   Listing of Instruments and channels evaluated. Polarization for conical MW SSMI/S and AMSR-E instruments are horizontal (H), vertical (V), and left-circular polarized (LCP)

Channel Number	Instrument						
	SSMI/S	AMSR-E	AMSU-A	AMSU-B	MHS	HIRS 3/4	AIRS
	Frequency in GHz					Wavelength microns	
1	50.3 V	6.925 H	23.8	89	89	14.95	324 channel subset
2	52.8 V	6.925 V	31.4	150	157	14.71	
3	53.596 V	10.65 H	50.3	183.3 +/- 1	183.311+/- 1	14.49	
4	54.4 V	10.65 V	52.8	183.3 +/- 3	183.311 +/- 3	14.22	
5	55.5 V	18.7 H	53.596	183.3 +/- 7	190.3	13.97	
6	57.29 LCP	18.7 V	54.4			13.64	
7	59.4 LCP	23.8 H	54.94			13.35	
8	150 H	32.8 V	55.5			11.11	
9	183.31 +/- 6.6 H	36.5 H	57.29			9.71	
10	183.31 +/- 3 H	36.5 V	57.29+/- .217			12.47	
11	183.31 +/- 1 H	89 H	57.29+/-.322+/-.048			7.33	
12	19.35 H	89 V	57.29+/-.322+/-.022			6.52	
13	19.35 V		57.29+/-.322+/-.010			4.57	
14	22.235 V		57.29+/-.322+/-.0045			4.52	
15	37 H		89			4.47	
16	37 V					4.45	
17	91.655 V					4.13	
18	91.655 H					4	
19						3.76	

The Advanced Microwave Sounding Unit A and B, and the Microwave Humidity Sounder (MHS) represent the three cross-track scanning MW instruments evaluated in this study. Each of these instruments was designed to measure the vertical structure of the Earth atmosphere, with the AMSU-B and MHS instruments particularly designed to obtain vertical moisture information. The remaining cross-track scanning instruments are the High-resolution Infrared Radiation Sounder (HIRS) versions 3 and 4, and the Atmospheric Infrared Radiation Sounder (AIRS). HIRS 3 and 4 utilize 19 channels to obtain vertical temperature and moisture structure within the Earth atmosphere.   Both instruments have a total of 20 channels that includes a visible channel; however, this visible channel was not evaluated in this study. The AIRS instrument is an atmospheric sounder with 2378 channels designed to obtain high-resolution vertical profiles of several atmospheric variables. A 324 channel subset was selected from a total of 2378 AIRS channels for initial evaluation.

D.   BLENDED PROFILES

Since the dropsondes from JET2000 only measured atmospheric variables below approximately 400 or 500 mb, data above the profiles was required to complete the atmospheric profile. Sufficient vertical extent is required to accurately depict the sensitivity to temperature and moisture for channels of interest. Temperature and moisture values above the dropsonde values were interpolated from the European Center for Medium-range Weather Forecasting (ECMWF) model analysis made available through the ECMWF data server at http://data.ecmwf.int/data/.

Values from the 0600, 1200, and 1800 UTC ECMWF analyses were used to interpolate both spatially and temporally to the JET2000 dropsonde locations and times. The ECMWF analyses have a horizontal resolution of 1.125 degrees and contain 23 vertical levels, extending up to the 1 mb pressure level. Linear interpolation in time and space between the ECMWF model grid points for 0600, 1200, and 1800 UTC analysis times was used to obtain values corresponding to the JET2000 dropsonde locations and drop times. The spatially interpolated analysis data were then used to construct a linear time trend between the 0600 UTC to 1200 UTC or 1200 UTC to 1800 UTC model values to interpolate in time the temperatures and moistures above the JET2000 dropsonde top value. It is assumed that the descent time between dropsonde launch and impact is negligible.

Each of the JET2000 dropsondes included header information that provides correction techniques for the variables and the respective accuracies of these measurements. At the top of each dropsonde profile, bad temperature data due to a lag caused by the adjustment to ambient conditions after the sonde was deployed from the aircraft were flagged with an error code. These bad data were removed from each dropsonde profile. The reported accuracy of the Vaisala RS-90 pressure measurements during the experiment was 0.4 mb between 100 mb and 1080 mb. To account for the dynamic effect of airflow past the dropsonde bulkhead a correction factor of 0.4 mb was added to each pressure measurement, as per the dropsonde header information.

The temperatures measured by the Vaisala RS-80 were corrected based on the fall rate of the dropsonde as it descended toward the surface, and these corrected temperatures are expected to be accurate to within 0.2 °C between -90 °C to 40°C. The corrected values were then compared with the ECMWF model profiles. The temperature adjustment of the ECMWF model values to blend smoothly with the dropsonde values was then made by calculating the difference between the ambient temperature measured at the highest JET2000 standard pressure level and the corresponding ECMWF pressure level. The standard level is defined as the highest dropsonde recorded level that matches one of the 23 analysis levels provided by the ECMWF. This level was either 500 mb or 600 mb depending on the level at which the dropsonde was deployed. Correction factors varied in magnitude from -0.21 °C to -0.37 °C (i.e., model was slightly too warm) on 28 August. The adjustment range for the measurements on 29 August ranged from -0.25 °C to +0.66 °C (model was slightly too cold).

A dry bias for the relative humidity (RH) measurements of the Vaisala RS-90 dropsondes was noted in the header information. However, the error is not consistent between sondes and no correction factor has been applied to the raw data. The accuracy of the RH data is reported to be 5% within the range 0% to 100%. The corresponding adjustment to the model relative humidity (RH) was performed by averaging the JET2000 RH values in the 500-600 mb layer and compared with the same layer average in the ECMWF data. The ratio JET2000 to ECMWF provides a percentage value to adjust the model profile above the highest JET2000 value. This correction factor was applied to the entire ECMWF profile above the JET2000 profile. The percentage values ranged from 29% to 75% (model was too moist) on 28 August. For the 29 August data, the percentage ranged from 50% to 96%.

The intent of blending the observed profiles with the ECMWF data is to provide a representative background state for the CRTM to use in calculating the brightness temperature for each respective sensor. In the following, "observed"

data will be considered as JET2000 data combined with the ECMWF data, unless otherwise specified. Figures 6, 7, 8 and 9 are examples of the blended profiles used in this study.
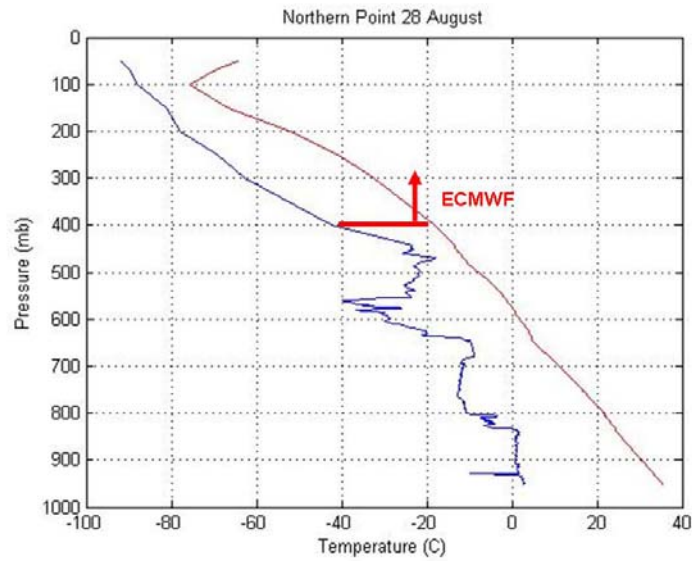
Figure 6.   Vertical profile of temperature and dewpoint for the northern point within the SAL air mass. Red line indicates the interface level between the ECMWF and JET2000 data.
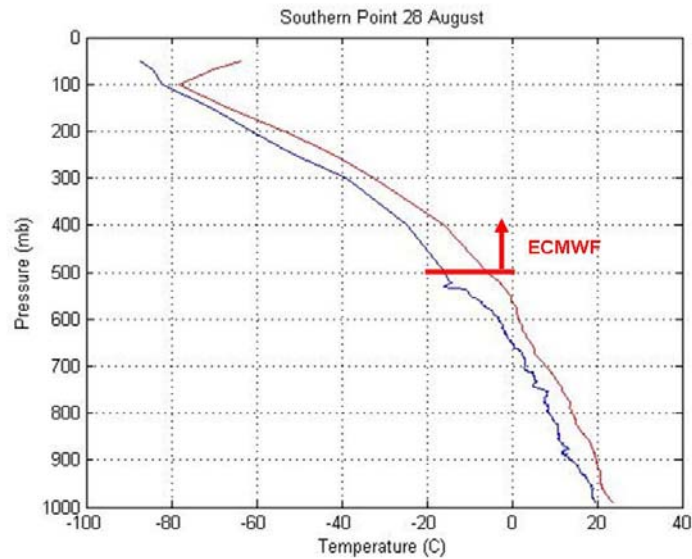
Figure 7.   As in Figure 6, except for the southern point within the non-SAL air mass.
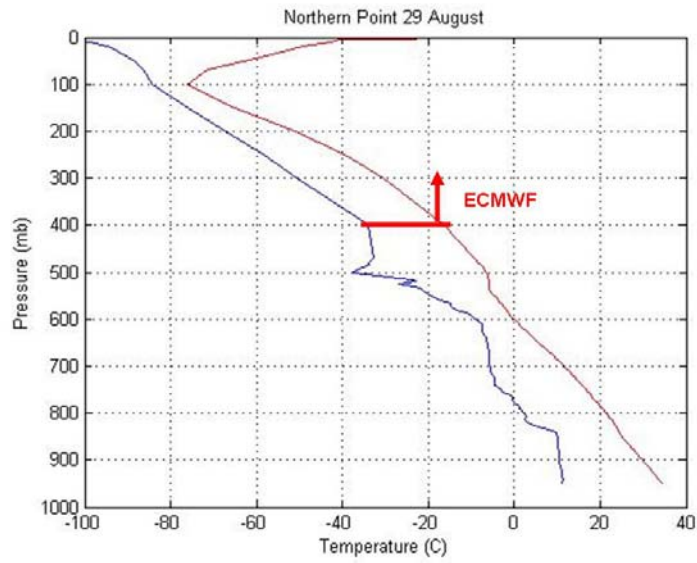
Figure 8.   As in Figure 6, except for 29 August.
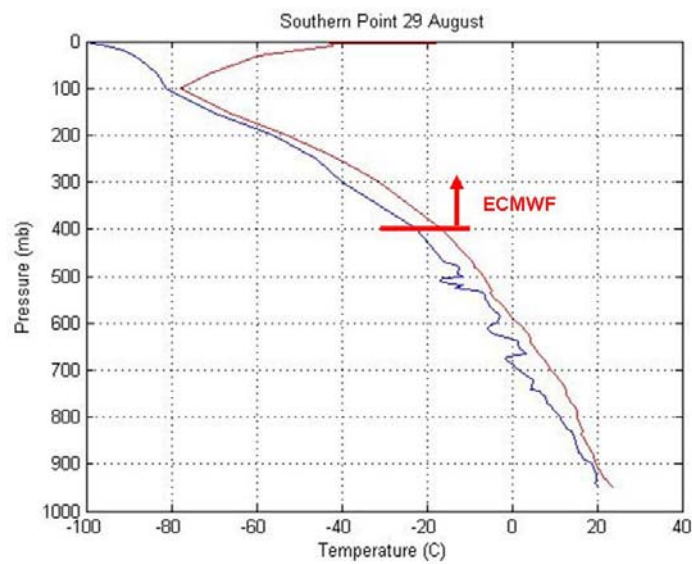
Figure 9.   As in Figure 7, except for 29 August.

THIS PAGE INTENTIONALLY LEFT BLANK

III. ANALYSIS

A. JET2000 OBSERVATIONS

The observed potential temperature, zonal wind, and humidity profiles from JET2000 flight 2 on 28 August are illustrated in Figure 10, and the observed potential temperature and zonal wind profile over the same region on 29 August are given in Figure 11. The hot, dry nature of the SAL is indicated by the weak vertical potential temperature gradient over the region north of 15 N. Convection in this region is characterized as being dry, with high potential for downburst activity. The influence of increasing equatorward moisture content allows for deep moist convection to occur. Lower-tropospheric temperatures to the south of the AEJ core are relatively cooler than those to the north, and then the temperature gradient reverses above the level of the AEJ.

On the 28 August flight (Figure 10), dropsondes were deployed in both air masses ahead of an approaching mesoscale convective system (MCS). On 28 August, the AEJ was located at approximately 650 mb over the region between 9 N to 11 N. During the 29 August flight (Figure 11), dropsondes sampled the post-MCS environment, in which marked changes had occurred in the structure of the AEJ from the previous day. After the passage of the MCS, the AEJ was split into two cores, with a portion of the jet easterly momentum transferred downward near the 900 mb pressure level presumably due to convective downdraft activity (Thorncroft et al. 2003).
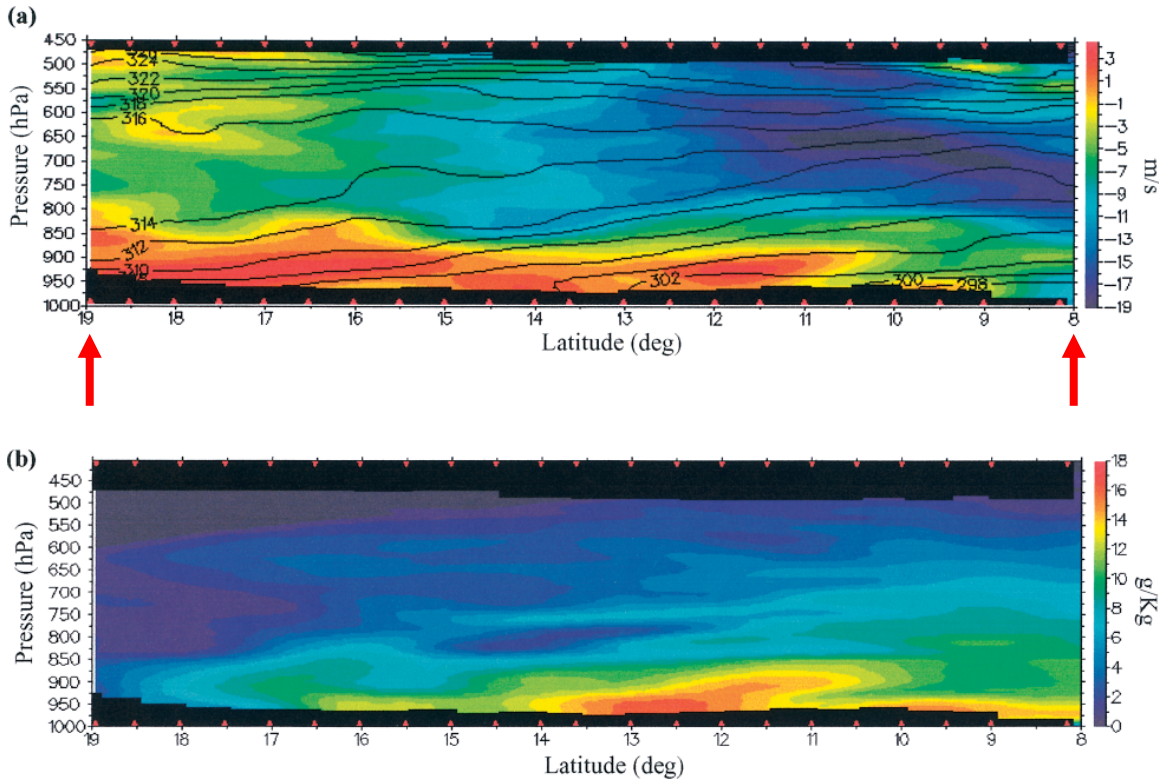
Figure 10.   Pressure-latitude cross-sections of (a) potential temperature (black lines) and zonal wind (shaded) and (b) humidity mixing ratio for flight 2 on 28 August.   The blackened regions along the top and bottom of the images denote the extent of the data coverage.   Red arrows indicate dropsonde locations input in the CRTM (After Thorncroft et al. 2003).
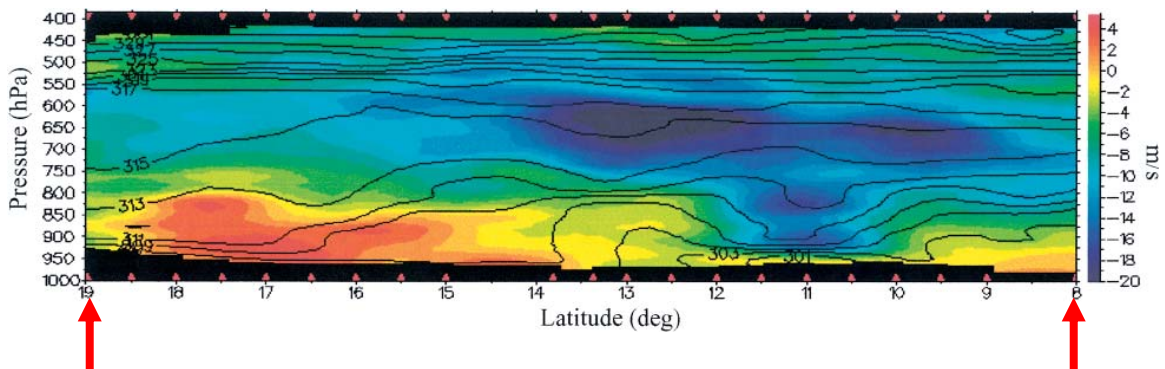
Figure 11.   As in Figure 10(a) above, except for flight 3 on 29 August. Notice the change in AEJ structure near 650 mb, in which the AEJ core has split into two distinct regions over 13.5 N and 10 N. Low-level wind structure has also modified from westerly to easterly between 28 August and 29 August (After Thorncroft et al. 2003).

B.   SIMULATIONS

Two simulated cases were examined to isolate the satellite instrument signal from the lower-tropospheric temperature and moisture gradients associated with the AEJ. These two simulated cases (Table 2) are intended to identify the ability of current satellite sensors to identify the gradients of moisture and temperature over the Sahel, both before and after the MCS propagated through the region. This signal was indicated by the brightness temperature (Tb) differences between the northern (19 N; SAL) and southern (8 N; non-SAL) ends of the JET2000 flights on 28 August and 29 August (arrows in Figures 10 and 11).   The Tb values were calculated by the CRTM using combinations of temperature (T) and specific humidity (q) vertical profiles that are different only below the AEJ level of 650 mb. A further description of each simulated case is given below. A third observed case was also evaluated to see if the results from the first two cases could be validated using realistic atmospheric and surface conditions.

Table 2.   Simulated and observed atmospheric profiles used to evaluate the sensitivity of satellite sensors to the AEJ moisture and temperature gradients. Case 1 was constructed to isolate the brightness temperature contribution from the moisture gradient, and Case 2 was constructed to isolate the brightness temperature contribution due to the temperature gradient. Case 3 is a brightness temperature difference between the observed SAL and non-SAL T and q gradients throughout the depth of the atmosphere rather than just below 650 mb.

CASE 1: Moisture Sensitivity with Average T(p) profile		Northern Point (SAL)	Southern Point (non-SAL)
Above 470/500 mb	ECMWF data	Avg q profile	Avg q profile
Above 650 mb	JET2000 data	Avg q profile	Avg q profile
Below 650 mb	JET2000 data	SAL q profile	Non-SAL q profile
CASE 2: Temperature Sensitivity with Average q(p) profile		Northern Point (SAL)	Southern Point (non-SAL)
Above 470/500 mb	ECMWF data	Avg T profile	Avg T profile
Above 650 mb	JET2000 data	Avg T profile	Avg T profile
Below 650 mb	JET2000 data	SAL T profile	Non-SAL T profile
CASE 3: Observed Sensitivity		Northern Point (SAL)	Southern Point (non-SAL)
Above 400/500 mb	ECMWF data	Model T(p), q(p)	Model T(p), q(p)
Below 400/500 mb	JET2000 data	Observed T(p), q(p)	Observed T(p), q(p)

The lower-tropospheric data from the JET2000 experiment were used in Cases 1 and 2 to provide realistic measurements of both the SAL and non-SAL

air masses.   Simulated profiles input to the CRTM for Cases 1 and 2 were provided at pressure levels between 1 mb and 950 mb with values provided at every 5 mb below the ECMWF/JET2000 data interface.   The original profiles were reduced to approximately 100 levels to normalize the number of data levels between the SAL and non-SAL cases so that the average temperature and moisture structure differences could be calculated.   This normalization also allowed different T and q profiles to be readily combined.   Another result of this normalization was the interface level between the JET2000 observations and the ECMWF data in Cases 1 and 2 was lower in the atmosphere than Case 3 as indicated in Table 2 above.   The Tb difference in Case 3 was evaluated using the entire dropsonde profiles obtained during the JET2000 experiment.

In all three cases it is assumed that the modeled satellite view is free of any clouds and aerosols, which is particularly important for IR and MW wavelengths that are sensitive to water vapor, cloud liquid water, and aerosol interactions.   The intent of this assumption is to provide results that could be used in a *best case* environment.   Also, a limitation of using the JET2000 data to construct the simulated profiles is that the experiment provides information for only two days over this specific region of interest.   However, it is assumed that the lower-tropospheric conditions observed during JET2000 are representative of the summer conditions over the Sahel.

C.   **SENSITIVITY EVALUATIONS WITH SIMULATED PROFILES**

The goal of this section is to identify which satellite channels were the most sensitive to the lower-tropospheric temperature and moisture gradients associated with the AEJ.   That is, the experiment was designed to use the Tb differences simulated by the CRTM to identify which channels had the largest response to perturbations in the lower-tropospheric temperature and moisture profiles.   The selected sensors were broken into conical- and cross-track scanning instruments for evaluation. The list of potential channels in Table 1 was first screened to remove channels whose primary sensitivity was to trace gases not modeled by the CRTM and those channels whose primary sensitivity was to atmospheric properties above 1 mb (steps one and two in Table 3).

The magnitude of the brightness temperature difference simulated in each of the cases was evaluated first as a way to determine if there was enough of a temperature or moisture gradient signal in the CRTM output for each respective satellite instrument channel. Those channels that indicated less than 1 K Tb difference were considered to not contain enough information to be useful for detecting the temperature and moisture gradients. These channels are removed in step three of Table 3. Each case was initially evaluated over a constant land surface for emissivity calculations. A grass-soil land surface type was initially used to define the surface properties with respect to the IR emissivity values. Channels removed in step four of Table 3, in which changes are made to the land surface type, will be described in Chapter III. F.

Table 3.   Channel list reduction steps used to remove selected channels from consideration. Each of these steps was applied to the simulated Cases 1 and 2 presented in Table 2.

Channel List Reduction Steps	
1	Remove channels exhibiting sensitivity to trace gases not modeled by the CRTM
2	Remove channels with sensitivity above the ECMWF model level top of 1 mb
3	Remove channels with simulated Tb difference of less than 1 K
4	Remove channels with simulated Tb difference of less than 1 K after emissivity perturbations

D.   MOISTURE SIGNAL: CASE 1

The objective in Case 1 was to isolate that portion of the brightness temperature difference due to changes in the lower-tropospheric moisture gradient between the SAL air to the north of the AEJ and the non-SAL air to the south of the AEJ. Thus, an average of the SAL and non-SAL temperature profiles was specified at all levels, and the specific humidity profile varied only below 650 mb. An average of the SAL and non-SAL specific humidity profiles was specified above the 650 mb level, so that the Tb signal is only due to the SAL and non-SAL humidity differences below 650 mb. In this way, the differences in the contribution of the lower-tropospheric moisture structure to the computed brightness temperature could be evaluated via the CRTM brightness temperature output. These Tb differences were calculated so that the non-SAL (moist) case is subtracted from the SAL (dry) case for each respective day, which results in most of the differences for the analyzed channels to be positive. The

moisture profiles provided to the CRTM to evaluate the moisture gradient for the 28 August and 29 August simulations are illustrated in Figures 12 and 13, respectively. The day-to-day differences, especially below 650 mb, highlight the change in the moisture gradient between the 28 August and 29 August flights due to the influence of the MCS moving through the region.
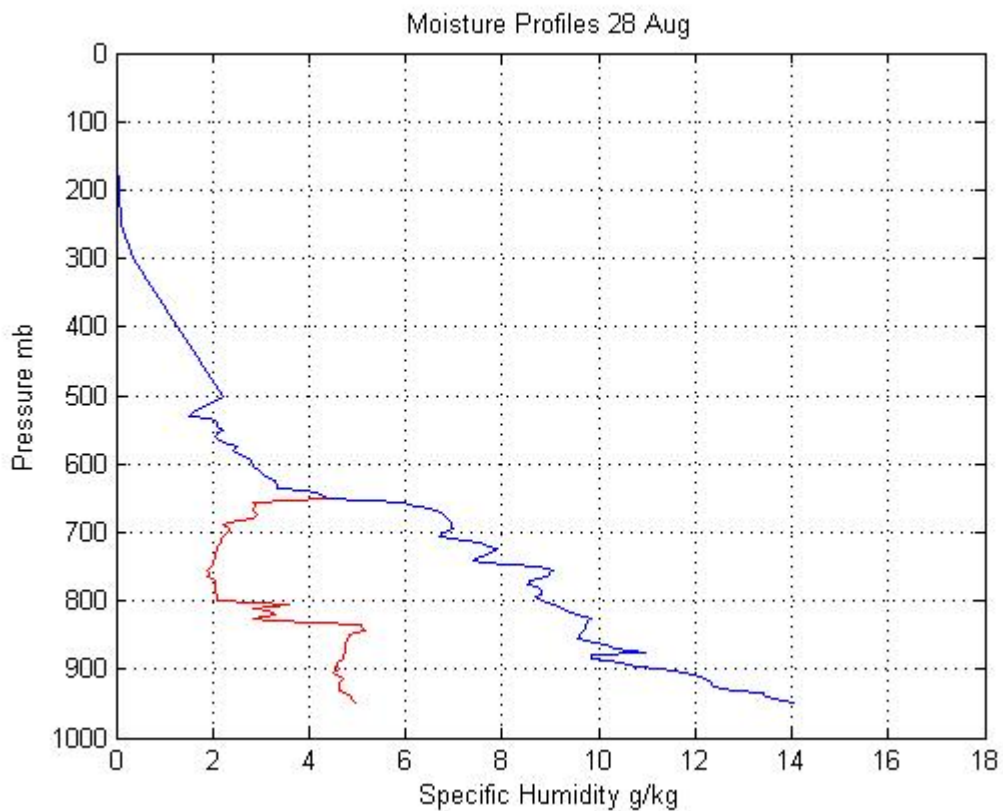
Figure 12.   Specific humidity profiles for the SAL (red) and non-SAL (blue) used to evaluate the moisture gradient across the AEJ on 28 August. Above the 650 mb level no differences are allowed between the two profiles.
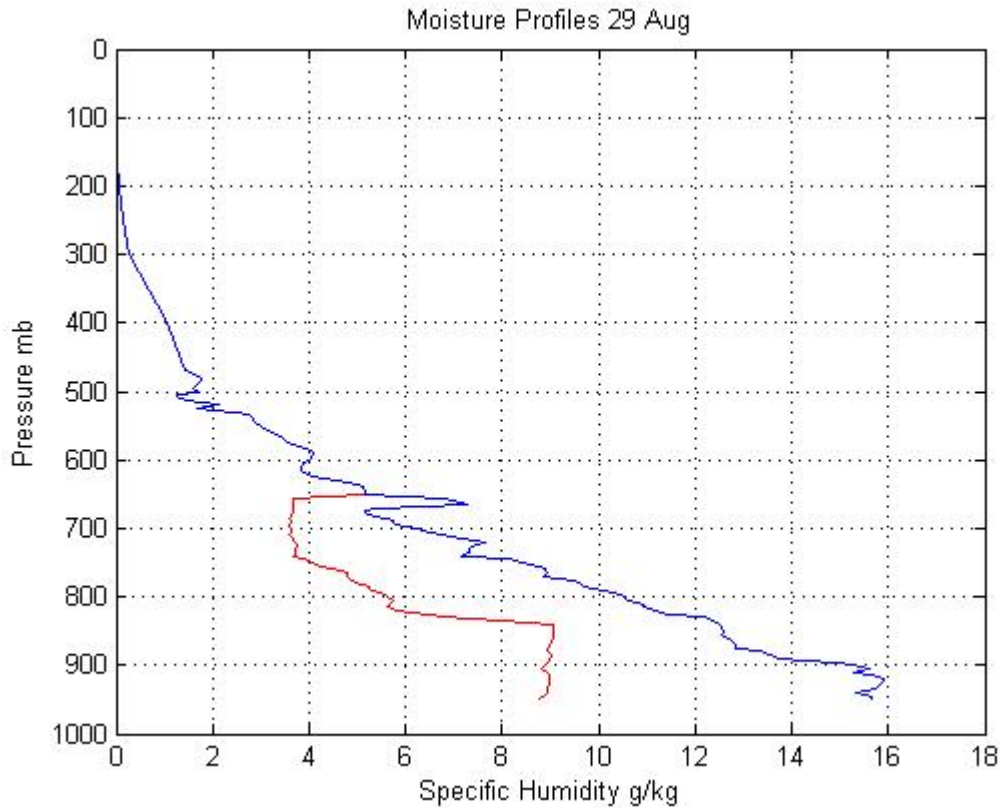
Figure 13.   As in Figure 12, except for 29 August. Note the overall decrease in moisture gradient below 650 mb relative to that in Figure 12.

1.   SSMI/S

The Defense Meteorological Satellite Program (DMSP) SSMI/S conical-scanning instrument was evaluated to reveal which of the sensor channels were the most sensitive to moisture perturbations below 650 mb. In step 2 of Table 3, channels 6 and 7 were removed because their sensitivity is well above the level of interest. The results for the remaining channels are presented in Figure 14. Those channels exhibiting sensitivity above the 1 K threshold on both days are: 19.35 GHz Vertical (V), 91.655 GHz Horizontal (H) and Vertical (V) polarization. Frequencies with a known sensitivity to water vapor (e.g., 22 and 183 GHz) had some sensitivity to the moisture perturbations, but not enough to pass the 1 K threshold. This small response is due to these channels having a majority of sensitivity above 650 mb. In all channels, day-to-day changes in the lower-tropospheric moisture gradient are revealed in the changes in Tb amplitude between 28 August and 29 August.

DMSP SSMIS Moisture Sensitivity

Figure 14.   SSMI/S brightness temperature differences due to only moisture perturbations below 650 mb for 28 August and 29 August.

An interesting result is the larger difference in the 150 GHz H channel in the 29 August case versus the 28 August case. This result can be explained by examining the CRTM Jacobian profile that indicates the magnitude of the change in Tb for a respective change in the state variable (Figure 15). A decrease in the Tb for a respective increase in water vapor is indicated by the negative sensitivity values, and an increase in the Tb value occurs for changes in those regions where positive sensitivity occurs. In other words, the change in the Tb value is a result of the integrated effect of the respective sensitivity multiplied by the change in the respective state variable. The 29 August Tb difference for the 150 GHz channel is caused by a 0.78 K higher SAL Tb compared to the 28 August case. Since the non-SAL Tb values for each day were within 0.03 K in magnitude, this increase in Tb can be explained by comparing the lower-tropospheric sensitivity to moisture and temperature. For the Jacobian with respect to moisture, the 29 August SAL case (Figure 15b) exhibits negative sensitivity (lower Tb) below

26

approximately 825 mb, while the negative response to moisture occurs near the 750 mb level in the 28 August SAL case (Figure 15a), and it is larger in magnitude overall. It should be noted that the resultant Tb is also dependent on the temperature Jacobian profile, which in the 29 August SAL case is larger in overall magnitude below 750 mb than the 28 August SAL case. This indicates a larger response to increases in temperature on 29 August compared to 28 August.
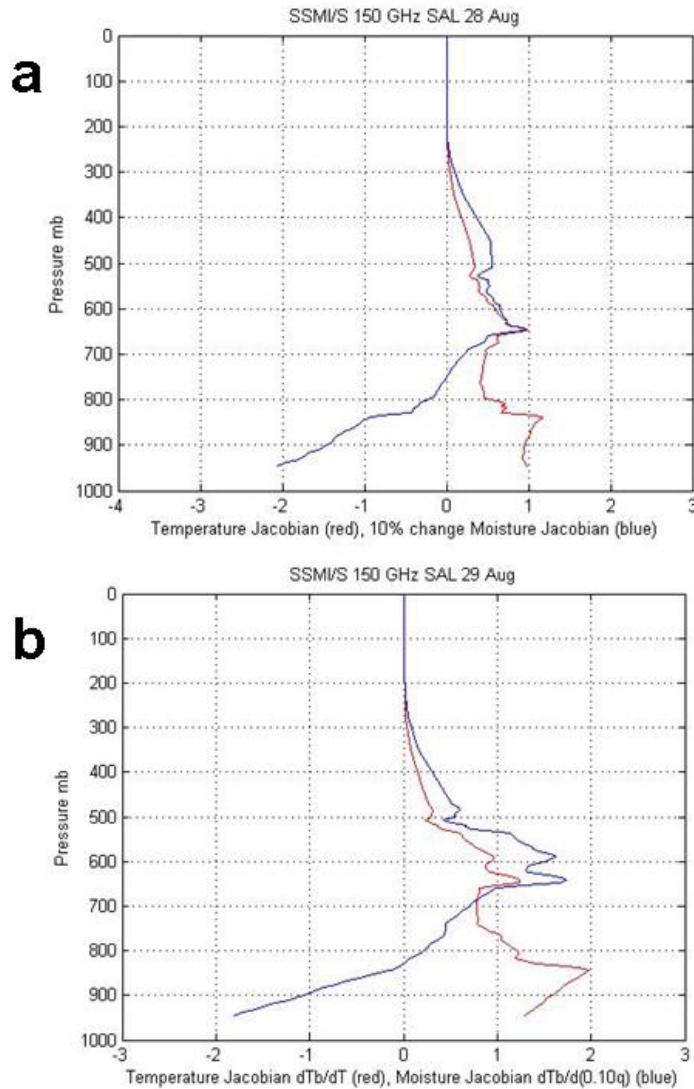
Figure 15. Jacobian profiles for the (a) SAL profile 28 August and (b) SAL profile 29 August illustrating sensitivity to changes in temperature (red) and a 10% change in moisture (blue) for the SSMI/S 150 GHz channel. Note the opposite Tb responses to the temperature versus moisture changes below 700 mb.

2.   AMSR-E

The other conical-scanning instrument evaluated in this study was the AMSR-E instrument on the NASA Aqua satellite (Figure 16). The strongest sensitivity to moisture perturbations was noted for 32.8 GHz V, and both the 89 GHz H and V polarizations. Each of these channels is a relative window channel, so that the 32.8 GHz channel is used to obtain surface temperature estimates. By contrast, the 89 GHz channels are primarily designed to sense low clouds and surface parameters (Pardo et al. 2007). As was the case with the SSMI/S instrument, differences in the moisture gradient can be detected for each day by all channels. However, only the larger moisture gradient in the 28 August profiles is consistently above the 1 K threshold. In all cases, a negative difference indicates a higher simulated Tb for the southern point in the non-SAL air mass. The Jacobian plots for the non-SAL air mass on 28 August (Figure 17a) and the SAL air mass on 28 August (Figure 17b) indicate the differences in sensitivity for the 89 GHz channel between the two air masses. Based on these plots, the effective differences in temperature and moisture sensitivity between the non-SAL (Figure 17a) and the SAL (Figure 17b) lead to the non-SAL air mass to return a simulated Tb value higher than that of the SAL.

Figure 16.   +AMSR-E brightness temperature differences due to only moisture perturbations below 650 mb for 28 August and 29 August.
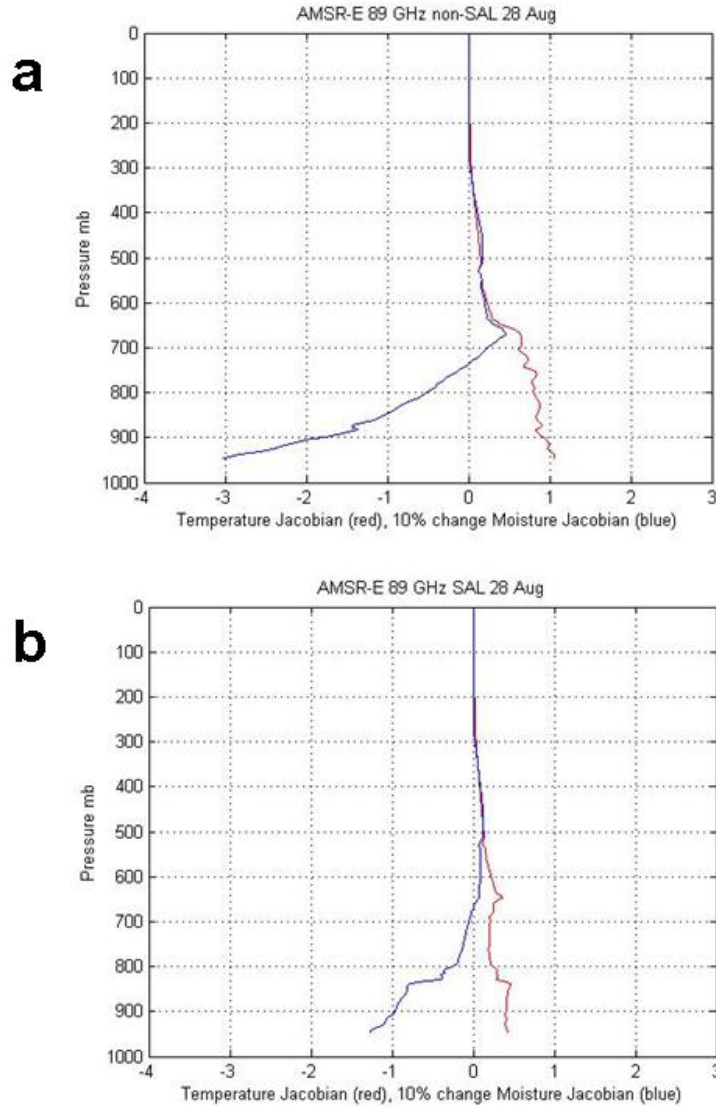
Figure 17.   Jacobian profiles as in Figure 15, except for the AMSR-E 89 GHz H channel (a) non-SAL profile 28 August and (b) SAL profile 28 August. Note the difference in sensitivity between the non-SAL and SAL air masses below 700 mb.

3.   AMSU-A

The AMSU-A instrument is a cross-track scanning sounding unit, and was simulated by the CRTM for a nadir view.   The sensitivities to moisture perturbations below 650 mb for the SAL and non-SAL air masses are illustrated in Figure 18. The 57.29 GHz channels 9-14 were removed from the evaluation due to sensitivity above the level of interest.   For the remaining channels, sensitivity above the 1 K threshold is noted only for the 89 GHz channel; this

30

sensitivity was slightly less in magnitude than that observed for the SSMI/S 91 GHz and AMSR-E 89 GHz channels. The magnitude of the moisture sensitivity for the AMSU-A 89 GHz channel indicates that the cross-track scanning instruments at nadir would not perform as well as the conical-scanning instruments.

NOAA AMSU A Moisture Sensitivity
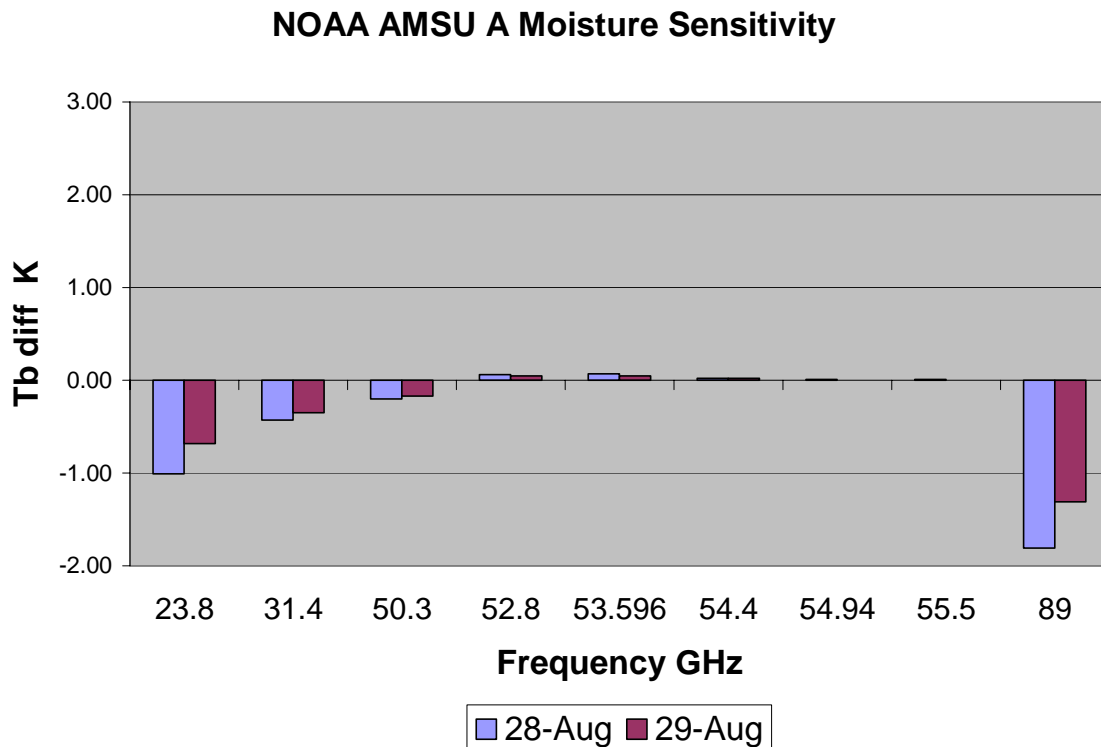
Figure 18.   AMSU-A brightness temperature differences due to moisture perturbations below 650 mb for 28 August and 29 August.

4.   AMSU-B and MHS

The AMSU-B has been in service since 1998 aboard the NOAA N-15 through N-18 satellites. The MHS instrument was launched aboard the N-18 satellite in 2005. Since the MHS was designed as a follow-on instrument to the AMSU-B series, both satellites will be discussed together in this section. The responses to the lower-tropospheric moisture perturbations are presented in Figure 19.
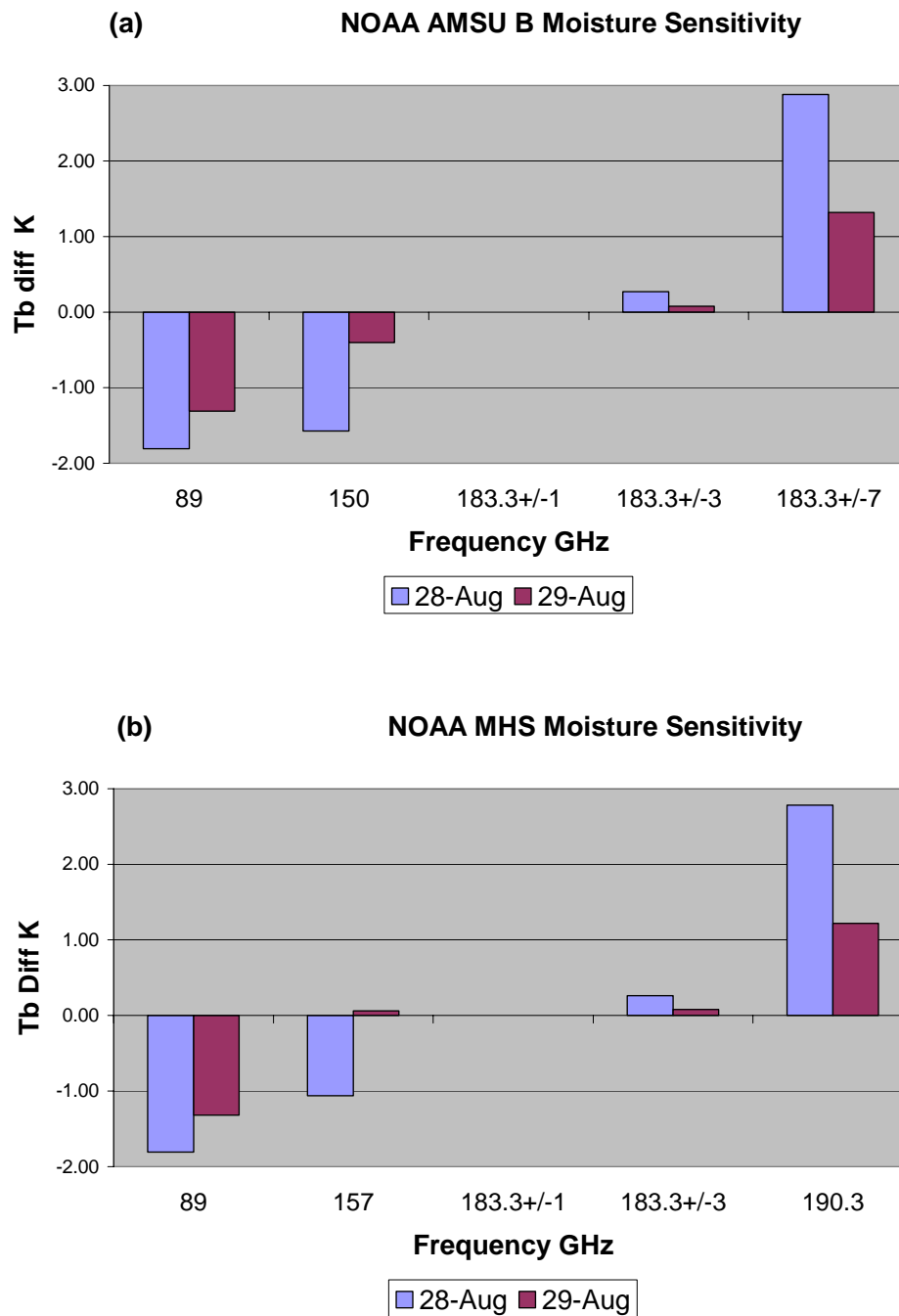
Figure 19.   AMSU-B and MHS brightness temperature differences due to moisture perturbations below 650 mb for 28 August and 29 August.

Both instruments have an identical sensitivity to simulated moisture perturbations for the 89 GHz channels. The responses for the AMSU-B 183.3+/-

7 GHz and the MHS 190.3 GHz channels are nearly identical, with the AMSU-B response 0.10 K larger than for the simulated MHS moisture gradient.

5. HIRS 3 and 4

The HIRS 3 instrument was designed with a field of view (FOV) of approximately 20 km while the HIRS 4 instrument has a 10 km FOV. Due to these similarities, both sensors will be discussed together. The Tb responses for the moisture sensitivity simulations for HIRS 4 are presented in Figure 20. Similar results were noted between HIRS 3 and 4, with HIRS 4 having a stronger response for each of the candidate channels. Channels 1, 2, and 10 (14.95, 14.71, and 12.47 microns, respectively) from both instruments, were removed from the initial evaluation due to a maximum sensitivity well above 650 mb.

HIRS 4 Moisture Sensitivty
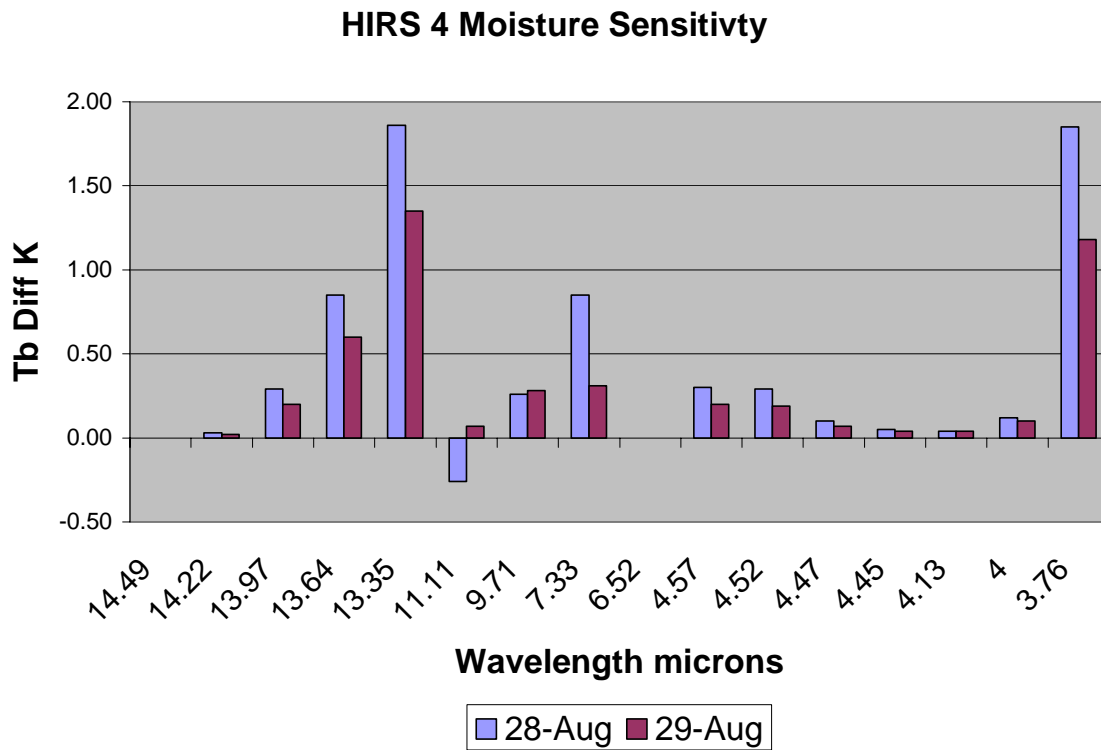
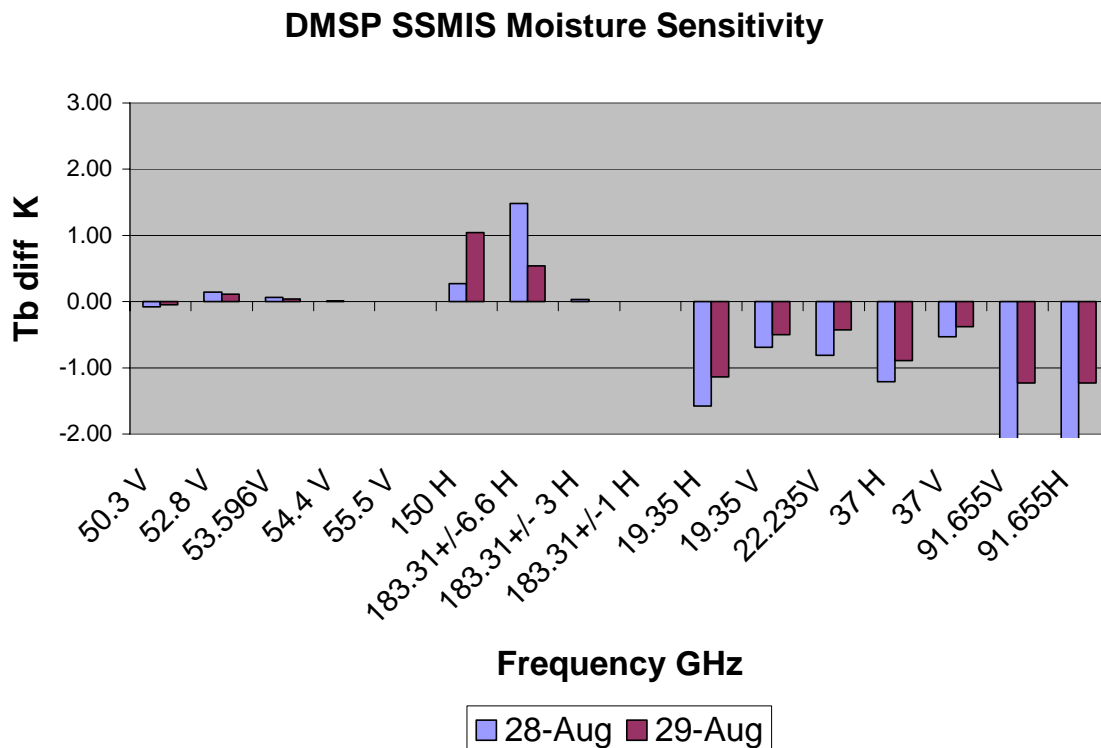
Figure 20. HIRS 4 brightness temperature differences due to moisture perturbations below 650 mb for 28 August and 29 August.

The largest response to moisture perturbations below the 650 mb level was found for the 13.35 micron and 3.76 micron channels on both HIRS 3 and 4. Traditional water vapor bands in the 6.52 and 7.33 micron channels did not show

sensitivity to the lower-tropospheric moisture gradients on 28 August and 29 August. This lack of response is explained by the higher water vapor absorption indicated by the IR transmittance diagram presented in Figure 4. The nonlinear effects of temperature on the 11.1 micron channels is indicated by the sign change from a negative Tb difference for the 28 August simulation to a positive Tb difference for the 29 August simulation. This result highlights that the moisture gradient below 650 mb was larger for the 28 August cases. The weaker moisture gradient in the 29 August cases is more influenced by the lower-tropospheric temperature profile. Recall that the average temperature profile for each day was constructed from that day's northern (SAL) and southern (non-SAL) points, so that these different average temperature profiles may also contribute to the Tb difference in sign and magnitude.

The HIRS 3 and 4 candidate channels are selected here based only on their respective sensitivity to changes in the moisture gradients below 650 mb. Additional effects of solar contamination on the 3.76 micron channel should be taken into account for operational use of this channel. The 13.35 micron channel also has sensitivity to carbon dioxide (CO_2) and ozone (O_3), neither of which is explicitly evaluated in this study. The CRTM does account for gaseous absorption due to CO_2 and O_3, but the effects studied here are related only to moisture gradient changes. Whereas CO_2 is generally regarded as being well mixed and homogeneous in the atmosphere, efforts are ongoing to assimilate trace gas effects into NWP models to help improve radiative transfer calculations (N. Baker, personal communication).

6. AIRS

The 324 channel subset for the AIRS sensor was used initially in this study to evaluate the performance of this instrument. A number of the AIRS 324 channel subset were subsequently not evaluated due either to their sensitivity to trace gases not accounted for by the CRTM, or to channel sensitivity above the upper-most level (1 mb) in this study (B. Ruston, personal communication). After

this initial reduction step, 115 AIRS channels were evaluated for their sensitivity to the moisture gradients and their changes for the 28 August and 29 August simulations.

The AIRS moisture gradient sensitivity results are presented in Figure 21. When compared to the HIRS 3/4 results, the AIRS instrument has a similar response to moisture in the 3 and 13 micron bands, but the AIRS water vapor bands near 7.5 microns have a much more significant response than the comparable HIRS water vapor channels. Presumably, this stronger response in the AIRS instrument is due to the higher spectral resolution relative to the HIRS instruments. In addition to the contamination issues for the 3 and 13 micron bands presented earlier, the 7.5-8 micron channels are in a region of variable amounts of CO_2 absorption, which is treated as a fixed gas by the CRTM.

NASA AIRS Moisture Sensitivty
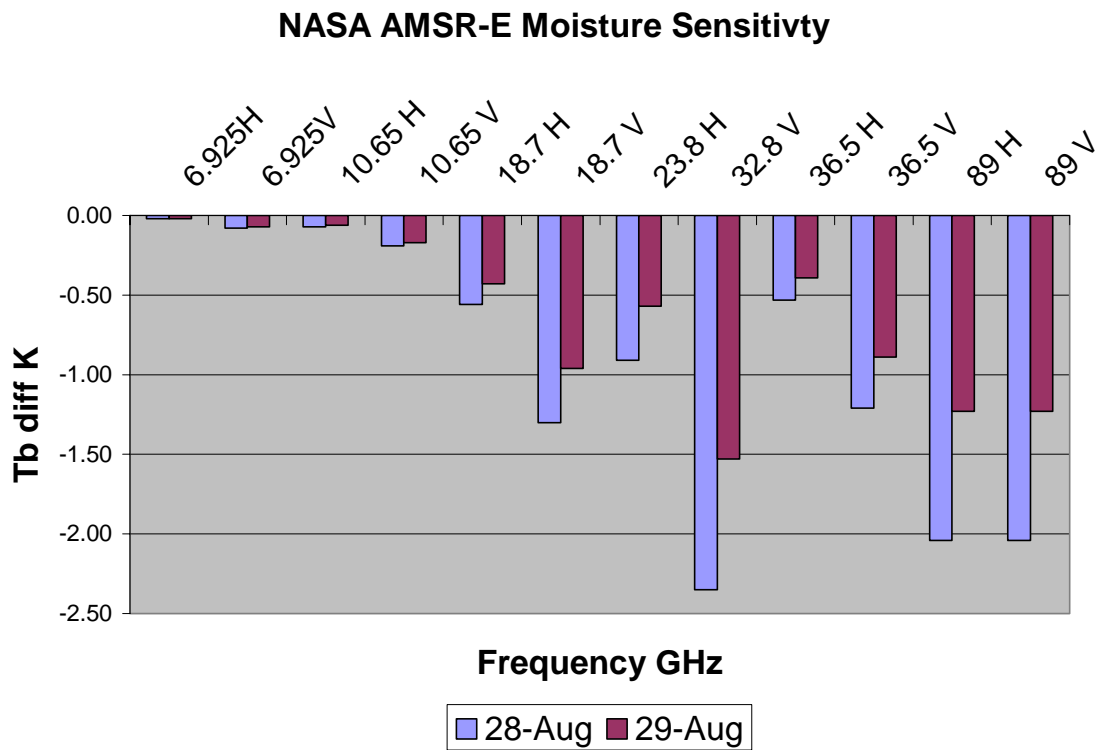
Figure 21.   AIRS brightness temperature differences due to moisture perturbations below 650 mb for 28 August and 29 August.

7.   Moisture Candidate Channels

Based on the results from the moisture sensitivity tests above, 32 (11 MW and 21 IR) candidate channels that have sensitivity above the 1 K threshold to moisture gradients for each simulated day (28 August and 29 August) are selected for further evaluation. These candidate channels are summarized in Table 4.

Table 4.   Candidate channels for detecting moisture gradients below the 650 mb level. AIRS channel numbers refer to the 324 channel subset.

Microwave Instruments			Infrared Instruments		
Instrument	Ch #	Channel	Instrument	Ch #	Channel
SSMI/S	12	19.35 H	HIRS 3/4	7	13.35
SSMI/S	17	91.655V	HIRS 3/4	19	3.76
SSMI/S	18	91.655H	AIRS	108	13.831
AMSR-E	8	32.8 V	AIRS	111	13.796
AMSR-E	11	89 H	AIRS	112	13.768
AMSR-E	12	89 V	AIRS	113	13.739
AMSU-A	15	89	AIRS	125	13.376
AMSU-B	1	89	AIRS	126	13.279
AMSU-B	5	183.3+/-7	AIRS	127	13.239
MHS	1	89	AIRS	128	13.165
MHS	5	190.3	AIRS	179	8.087
			AIRS	181	7.991
			AIRS	182	7.779
			AIRS	183	7.742
			AIRS	190	7.513
			AIRS	313	3.835
			AIRS	316	3.813
			AIRS	318	3.791
			AIRS	321	3.775

For each of the MW instruments analyzed, the response to moisture perturbations was largest for window channels that have greater sensitivity in the lower troposphere. With respect to the water vapor bands near 183 GHz, each instrument has a similar pattern with the largest response for the channels that have sensitivity in the lowest portion of the atmosphere. A comparison between the SSMI/S 183.3+/-6.6 GHz H, the AMSU-B 183.3+/-7 GHz, and the MHS 190.3 GHz channels reveals that the strongest response to the simulated moisture

36

perturbations below 650 mb is found with the AMSU-B 183.3+/-7 GHz channel. The larger sensitivity exhibited by AMSU-B is attributed to the shorter path length inherent in the cross-track scanning instruments at nadir versus conical-scanning instruments at a 53.1 degrees satellite inclination angle.

For the IR spectrum, the strongest response was found for the AIRS water vapor absorption channels. In particular, the largest response was in the 7.513 micron channel. For the HIRS 3/4 water vapor channels, neither the 6.52 or 7.33 micron channels indicated significant sensitivity (above 1 K) in the Tb difference between the northern (SAL) and southern (non-SAL) points evaluated.   The nearest wavelengths on the AIRS (6.56 and 7.314 microns) instrument also indicated a low sensitivity to moisture perturbations similar to the HIRS 3/4 results.

E.   TEMPERATURE SIGNAL: CASE 2

The objective of Case 2 in Table 2 is to isolate the temperature contribution below 650 mb to the Tb difference between the northern (SAL) and southern (non-SAL) points.   In this case, the specific humidity profile is an average of the SAL and non-SAL specific humidity profiles from the 28 August and 29 August ECMWF and JET2000 blended profiles.   A similar average temperature profile, down to the 650 mb level, was used in the Case 2 simulations.   Below this level, the JET2000 observed SAL and non-SAL temperature profiles were used to estimate the changes in Tb differences due only to those changes in the lower-tropospheric temperature structure. This low-level baroclinicity is responsible for the location and intensity of the AEJ. Similar in construct to the moisture gradient in Case 1, the temperature results were calculated as SAL minus non-SAL to maintain consistency and yield mostly positive difference results.

In each of the simulations, the surface level is defined as the 950 mb level. The magnitude of the 950 mb temperature gradient for the 28 August simulation is approximately $13°C$, and the 29 August gradient strength decreases to just over $9°C$. In addition to identifying which channels can consistently observe the lower-tropospheric temperature gradient, results from Case 2 will also

demonstrate which satellite instrument channels can detect this day-to-day change in the strength of the temperature gradient below 650 mb. In each of the cases below, channels with sensitivity to trace gases not modeled by the CRTM and sensitivity to levels above the ECMWF model top of 1 mb have been removed from consideration. The temperature values provided to the CRTM to evaluate the temperature gradients for the 28 August and 29 August simulations are given in Figures 22 and 23, respectively.
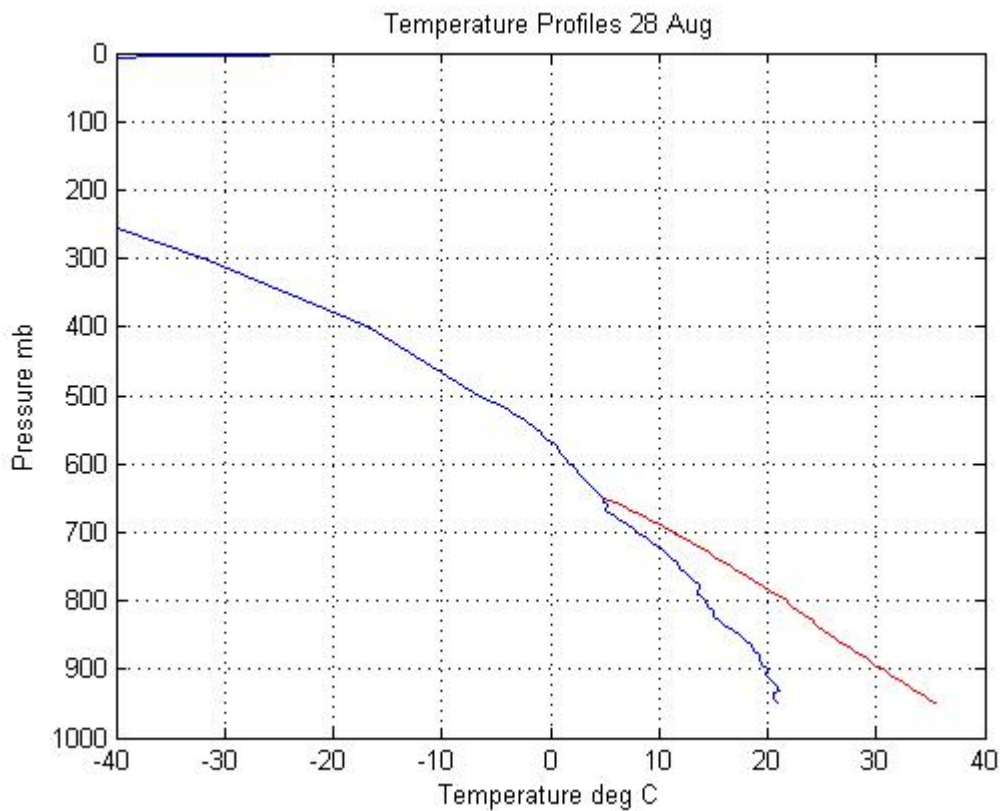
Figure 22. Temperature profiles for the SAL (red) and non-SAL (blue) used to evaluate the temperature gradient across the AEJ on 28 August. The temperatures do not vary above 650 mb in the Case 2 simulations.
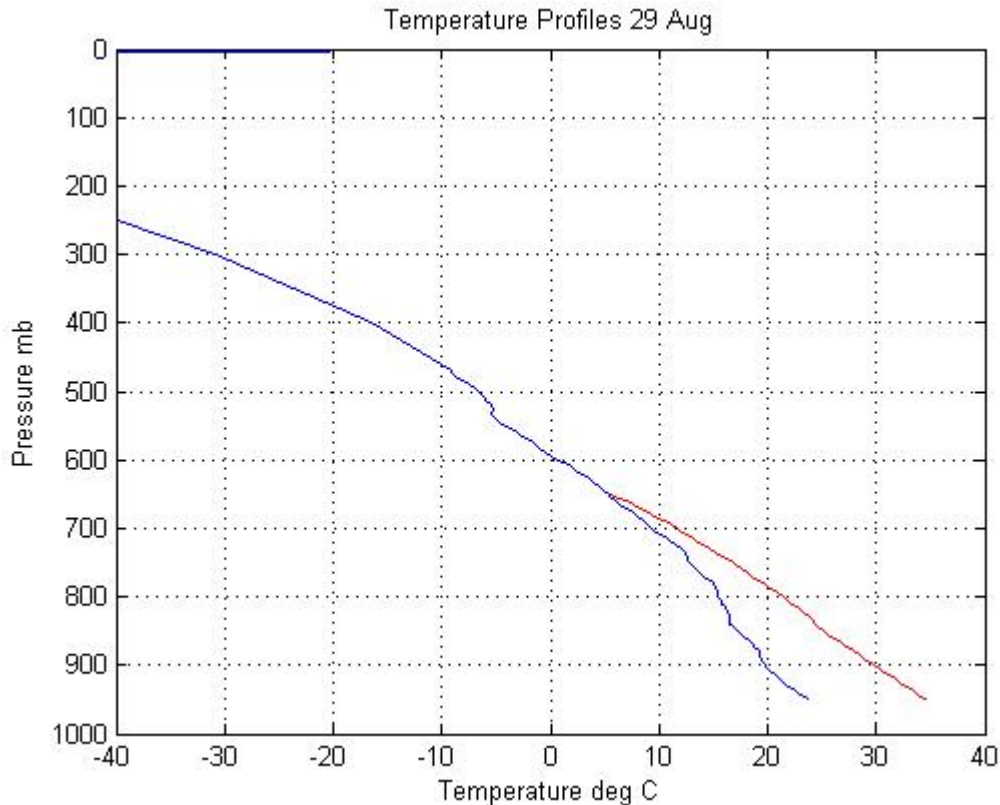
Figure 23.   As in Figure 22, except for 29 August.   The surface temperature gradient has weakened compared to the 28 August gradient.

1.   SSMI/S

Several of the SSMI/S channels have a large sensitivity to the temperature gradient below 650 mb (Figure 24). In step 2 of Table 3, channels 6 and 7 were removed because their sensitivity is well above the level of interest. A sense of the sounding nature of channels 1-5 (50-55 GHz) is apparent due to the consistent decrease in magnitude with increasing frequency. These frequencies are in a region of increasing oxygen (O2) absorption. Of these channels, the 50.3 GHz V channel has the largest sensitivity to the temperature perturbations, and it is concluded that this channel has the most sensitivity to the lowest portion of the atmosphere versus the other oxygen absorption channels. Sensitivity is also noted for the 150 GHz H window channel, as well as 19-91 GHz channels in Figure 24. Sensitivity due to polarization changes were noted for the 19.35 GHz and 37 GHz frequencies, with the vertically polarized signal approximately 0.4-0.5 K larger in both cases relative to the corresponding horizontally polarized

signal. This polarization difference does not appear for the 91.655 GHz channels, with identical Tb difference values for both the vertically and horizontally polarized channels.
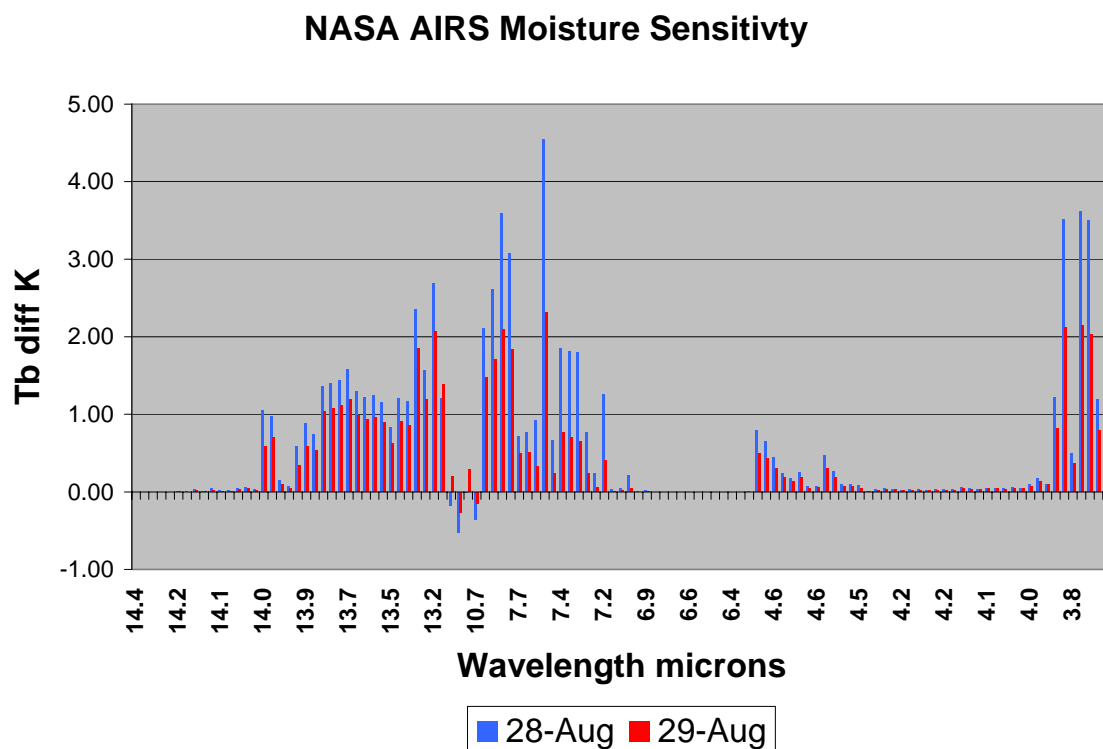
DMSP SSMIS Temperature Sensitivity

Figure 24. SSMI/S brightness temperature differences due to temperature perturbations below 650 mb for 28 August and 29 August.

2. AMSR-E

All of the AMSR-E channels have a strong response to the temperature perturbations imposed in Case 2 (Figure 25). Each of the channels evaluated has sensitivity well above the 1 K threshold, with the largest Tb differences noted for the lowest frequency channels 1-4 (6.925-10.65 GHz). Of the MW instrument channels analyzed, these channels have the lowest frequencies evaluated and they have the highest transmittance values as illustrated in Figure 5. This makes AMSR-E channels 1-4 the best atmospheric windows to detect the changes in the Earth surface properties. Typically, these channels are used to derive

surface properties over the ocean, since the nature of land surface emissivity is more variable (Pardo et al. 2007). This effect will be studied further in Chapter III. F.

NASA AMSR-E Temperature Sensitivity

Figure 25. AMSR-E brightness temperature differences due to temperature perturbations below 650 mb for 28 August and 29 August.

3. AMSU-A

AMSU-A channels 3-8 (50-55 GHz) have the same type of response (Figure 26) to the temperature perturbations below 650 mb as previously noted with the similar frequencies on the SSMI/S instrument (Figure 24). Although channel 1 (23.8 GHz) is typically used as an atmospheric water vapor sounding channel (English 2004), a strong response to temperature is noted in this temperature gradient simulation. This is another indication of the impact of temperature on the Tb output for water vapor channels. The largest response to the lower-tropospheric temperature perturbations occurs with the 31.4 GHz channel, which is an atmospheric window channel typically used for temperature measurements (Pardo et al. 2007).

41

NOAA AMSU ATemperature Sensitivity

Figure 26.   AMSU-A brightness temperature differences due to temperature perturbations below 650 mb for 28 August and 29 August.

A similar, but slightly less pronounced response is found with the 89 GHz channel as well (Figure 26). An advantage of the 31.4 GHz channel is that it would be less susceptible to cloud impacts than the 89 GHz channel, due to the 31.4 GHz channel's longer wavelength relative to cloud particle size. In each of the simulations, it is assumed that the environment is cloud-free, but the moist-convective environment that characterizes the non-SAL air mass is often cloud-contaminated from a remote sensing perspective.

4.   AMSU-B and MHS

Similar to the Case 1 results presented in Chapter III. D earlier, the AMSU-B and MHS results will be presented together due to their similarities in channel frequencies. The lower-tropospheric temperature simulations for the AMSU-B and MHS sensors are presented in Figure 27.

(a) **NOAA AMSU-B Temperature Sensitivity**

(b) **NOAA MHS Temperature Sensitivity**
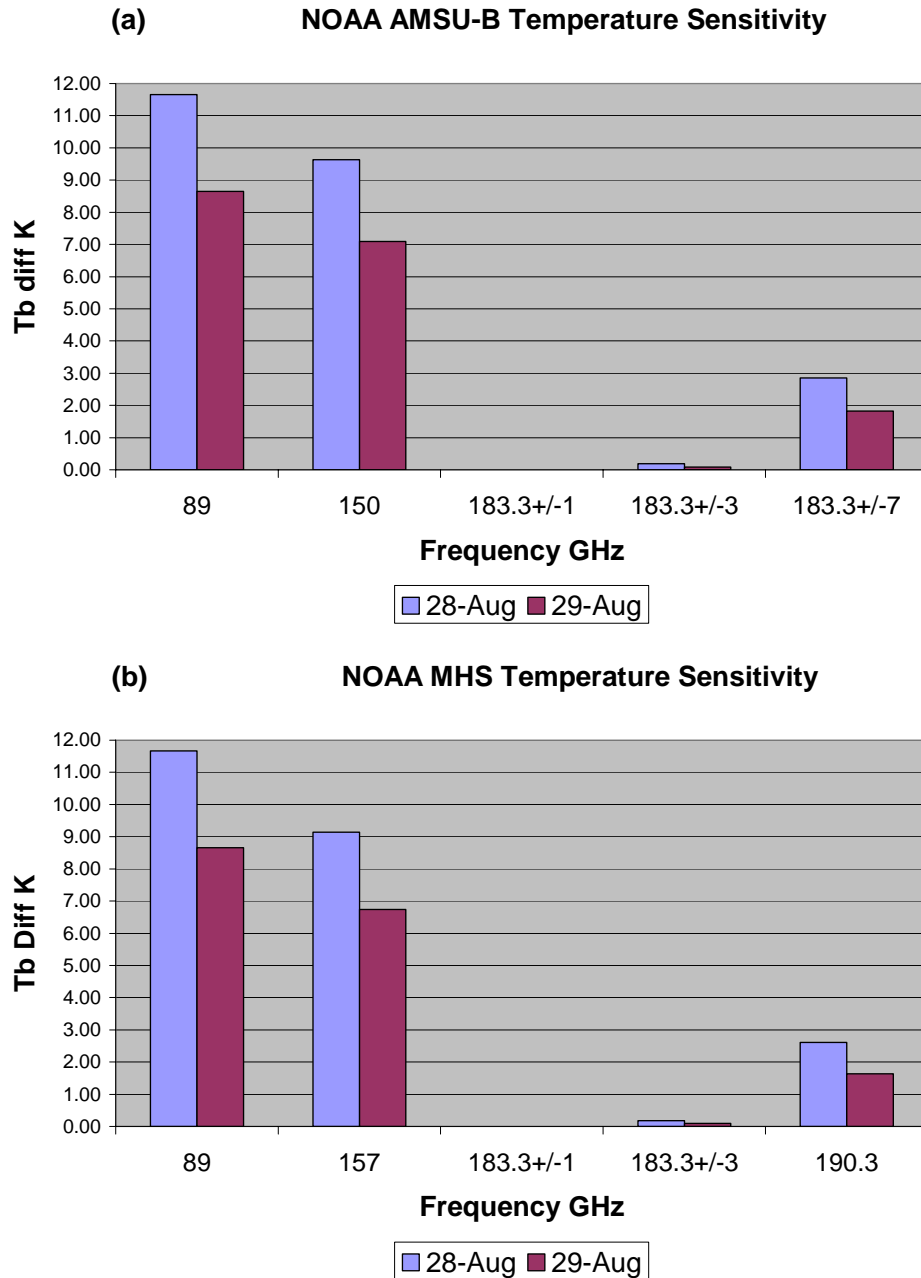
Figure 27.   (a) AMSU-B and (b) MHS brightness temperature differences due to temperature perturbations below 650 mb for 28 August and 29 August.

For both instruments, sensitivity well above the 1 K threshold is apparent for the 89 GHz, 150 GHz (AMSU-B), 157 GHz (MHS), 183.3+/-7 GHz (AMSU-B), and the 190.3 GHz (MHS) GHz channels. The moisture profiles in Case 2 simulations are constant to isolate the contribution due to the lower-tropospheric

temperature gradients only.   Slight differences in sensitivity are apparent between the 150 GHz AMSU-B channel and the MHS 157 GHz channel, with the former channel response approximately 0.4-0.5 K more sensitive (larger magnitude difference) than the latter.

5. HIRS 3 and 4

Only the HIRS 3 instrument will be presented (Figure 28) since the differences between the HIRS 3 and 4 instruments were not very large.   The HIRS 4 instrument was slightly more sensitive than the HIRS 3 for channels 6-8 (11-13 microns) by as much as 0.69 K.   For the shortwave IR, the HIRS 3 instrument was slightly more sensitive than HIRS 4 for channels 13-16 (4.57-4.45 microns) by as much as 0.86 K.   Although the largest sensitivity was for the 9.71 micron channel, this channel is known to be sensitive to O_3 absorption, which was not evaluated in this study.   Strong responses to temperature perturbations were noted for the longwave IR channels 11.1-13.6 microns.   Another peak of sensitivity is noted in the CO_2 absorption window in the shortwave IR bands. The sounding capability of the HIRS instruments is apparent due to the progressive decrease in sensitivity as the CO_2 absorption increases between 4.57 and 4.45 microns, as absorption makes the atmospheric signal more opaque with respect to the lower-tropospheric temperature perturbations.
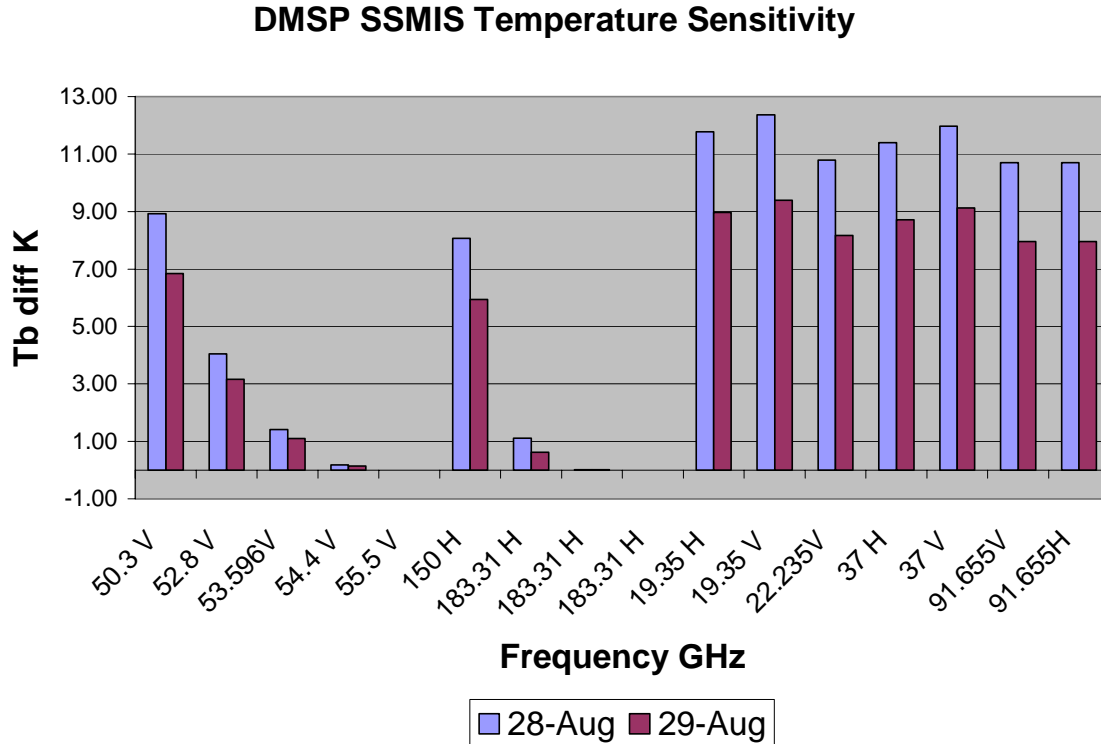
HIRS 3 Temperature Sensitivity
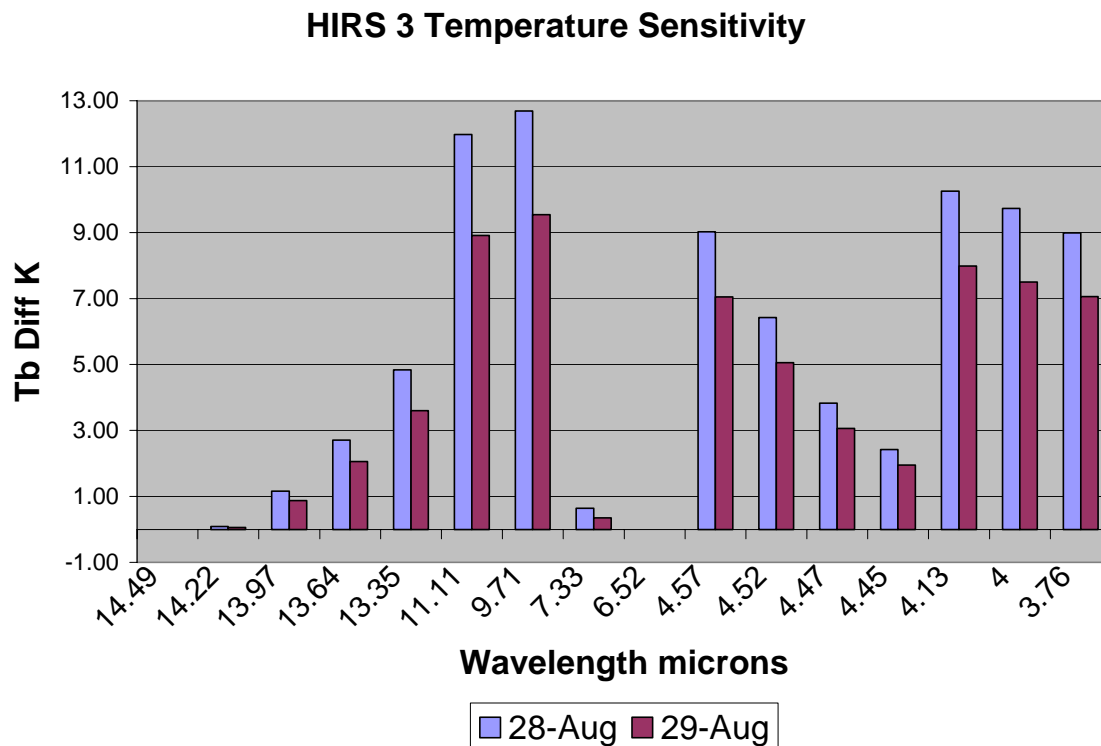
Figure 28.   HIRS 3 brightness temperature differences due to temperature perturbations below 650 mb for 28 August and 29 August.

6.   AIRS

The results for the temperature perturbations imposed in Case 2 for the selected 115 AIRS channels analyzed are presented in Figure 29.   The overall response is similar to that of the HIRS instruments, with the most significant sensitivity (above 8 K Tb difference) concentrated in the 11-13 micron bands. Secondary sensitivity maxima occur in the shortwave IR below 4.584 microns. A significant peak in the water vapor absorption band occurs for the 7.513 micron channel, which indicates the non linear contribution of temperature and water vapor to the Tb output is not alleviated through the high spectral resolution of the AIRS instruments. The AIRS results also reveal that this instrument can see not only the individual gradients of temperature for the 28 August and 29 August simulations, but it can also discriminate the changes in magnitude of these respective gradients. The largest sensitivity to this day-to-day change occurs in the longwave IR channels near 11 microns and in the shortwave IR near 4 microns.

NASA AIRS Temperature Sensitivity

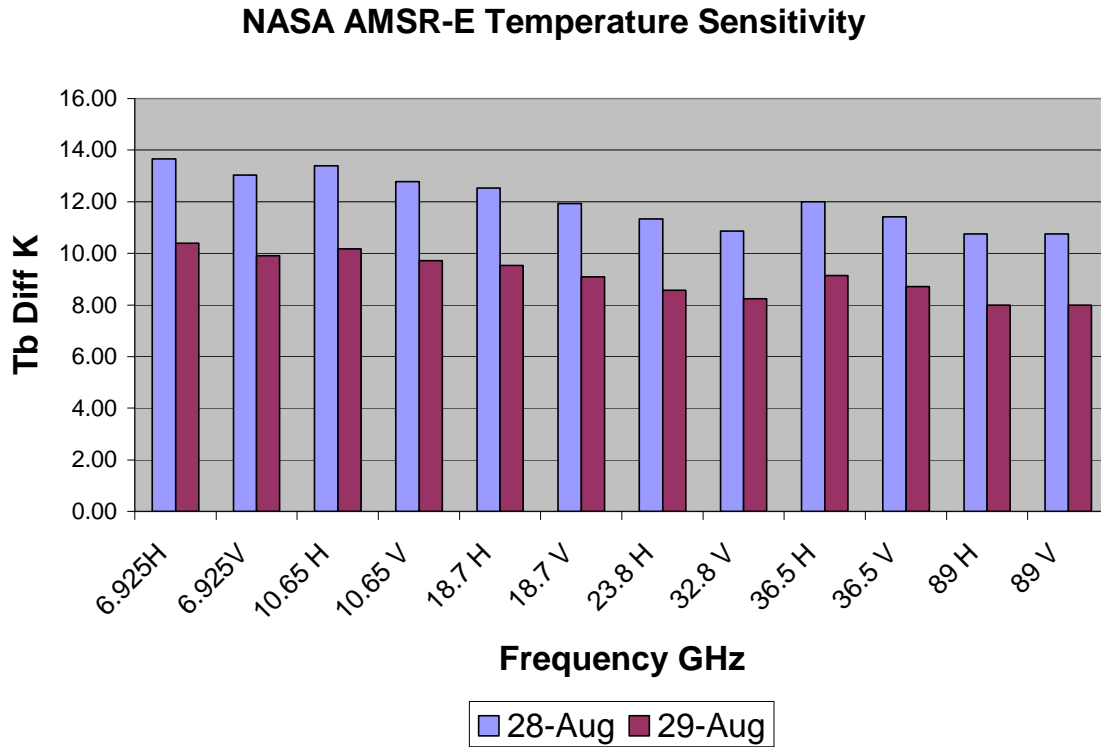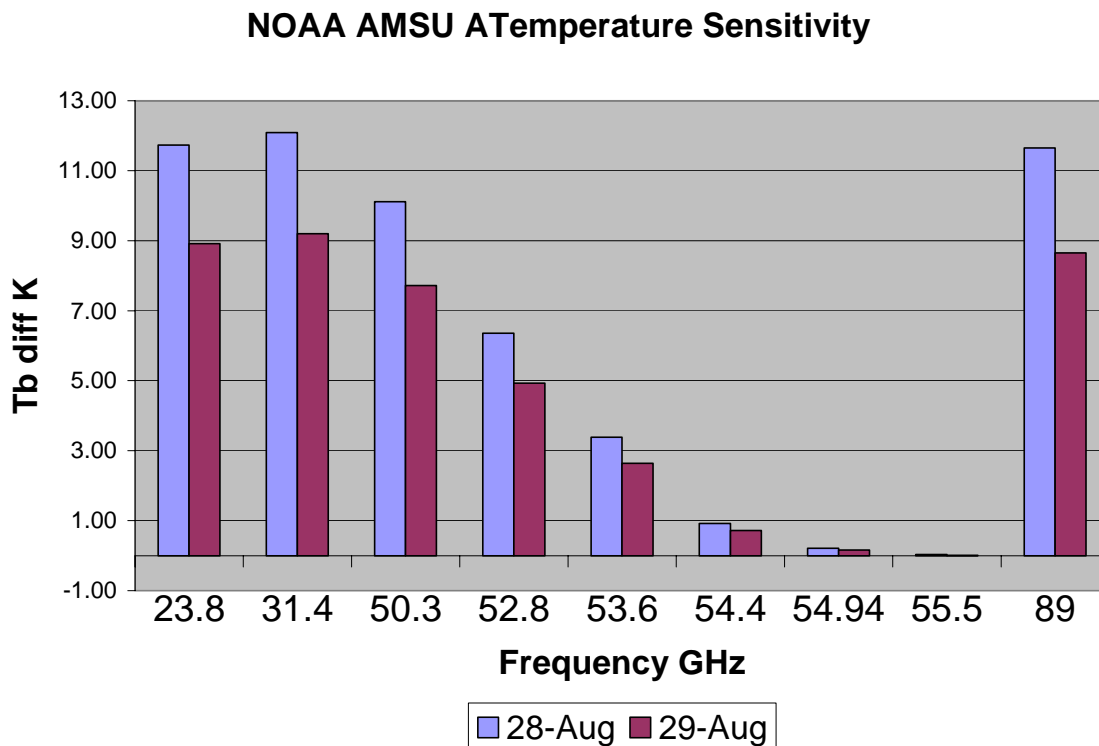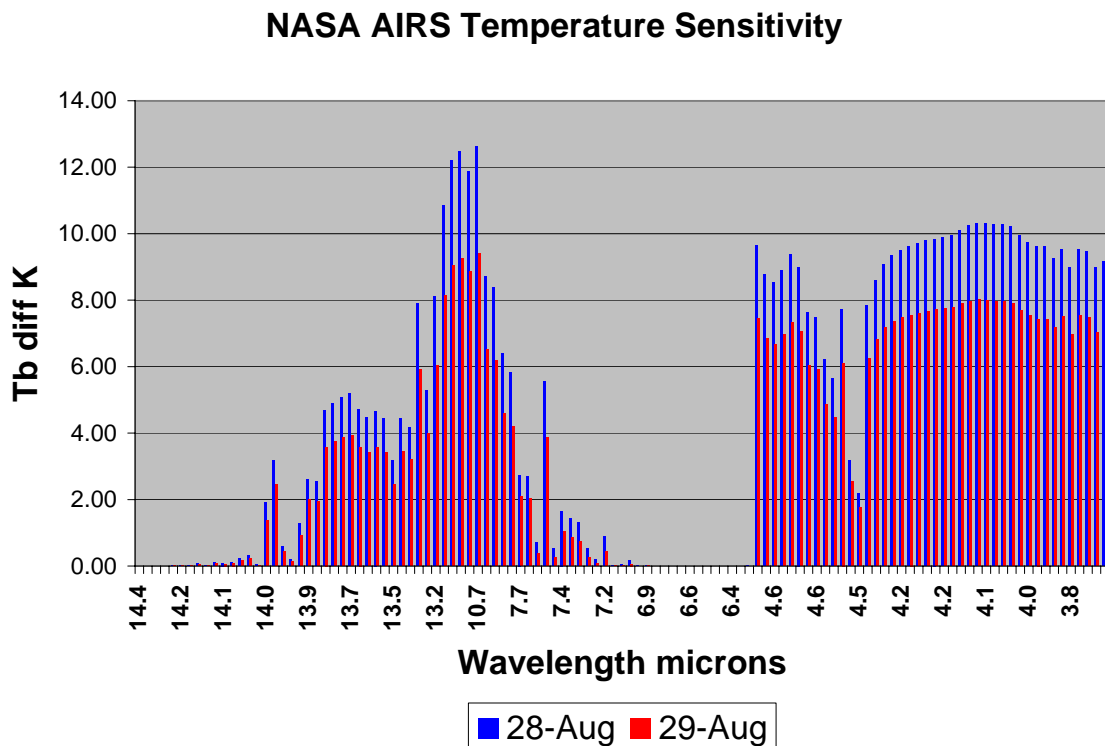Figure 29.   AIRS brightness temperature differences due to temperature perturbations below 650 mb for 28 August and 29 August.

7.   Temperature Candidate Channels

Those channels that indicated at least a 1 K Tb difference for both the 28 August and 29 August simulations for Case 2 are presented in Tables 5 and 6 below for the MW and IR instruments, respectively. From all of the MW channels analyzed, 35 were selected as candidates for further evaluation. In the IR, 95 channels were considered to have the desired sensitivity in these temperature gradient simulations. These channels are considered the candidate channels for temperature gradient structure related to the location and intensity of the AEJ, and will be the basis for further evaluations in Chapter III. F.

Table 5.   Candidate MW channels for detecting temperature gradients below the 650 mb level. AIRS channel numbers refer to the 324 channel subset.

Microwave Instruments								
Instrument	Ch #	Channel	Instrument	Ch #	Channel	Instrument	Ch #	Channel
SSMI/S	1	50.3 V	AMSR-E	1	6.925H	AMSU-A	1	23.8
SSMI/S	2	52.8 V	AMSR-E	2	6.925V	AMSU-A	2	31.4
SSMI/S	3	53.596V	AMSR-E	3	10.65 H	AMSU-A	3	50.3
SSMI/S	8	150 H	AMSR-E	4	10.65 V	AMSU-A	4	52.8
SSMI/S	12	19.35 H	AMSR-E	5	18.7 H	AMSU-A	5	53.596
SSMI/S	13	19.35 V	AMSR-E	6	18.7 V	AMSU-A	15	89
SSMI/S	14	22.235V	AMSR-E	7	23.8 H	AMSU-B	1	89
SSMI/S	15	37 H	AMSR-E	8	32.8 V	AMSU-B	2	150
SSMI/S	16	37 V	AMSR-E	9	36.5 H	AMSU-B	5	183.3+/-7
SSMI/S	17	91.655V	AMSR-E	10	36.5 V	MHS	1	89
SSMI/S	18	91.655H	AMSR-E	11	89 H	MHS	2	157
			AMSR-E	12	89 V	MHS	5	190.3

Unlike the moisture evaluations in Chapter III. D, the sensitivity to temperature perturbations in the lower troposphere revealed several candidate MW channels in the lower frequency region below 32 GHz that will not be as susceptible to cloud contamination as those in the 37 GHz and higher frequencies. This cloud-contamination aspect is especially important for remote sensing of the atmosphere below 650 mb over the area to the south of the AEJ typically characterized by moist convection and cloud contamination.

One aspect not explicitly examined in this study is the impact of horizontal resolution on the respective Tb differences for each sensor and individual channels. A trade-off exists for the lower frequency MW channels that have less cloud impacts but poorer horizontal resolution compared to the higher frequency channels that have larger cloud impacts but better horizontal resolution. The impacts of these tradeoffs should be studied further to evaluate the actual usefulness of these candidate channels.

Table 6. Candidate IR channels for detecting temperature gradients below the 650 mb level. AIRS channel numbers refer to the 324 channel subset.

Infrared Instruments											
Instrument	Ch #	Channel	Instrument	Ch #	Channel	Instrument	Ch #	Channel	Instrument	Ch #	Channel
HIRS 3/4	6	13.64	AIRS	99	14.002	AIRS	181	7.991	AIRS	291	4.174
HIRS 3/4	7	13.35	AIRS	101	13.968	AIRS	182	7.779	AIRS	292	4.172
HIRS 3/4	8	11.11	AIRS	106	13.854	AIRS	183	7.742	AIRS	293	4.17
HIRS 3/4	9	9.71	AIRS	107	13.848	AIRS	184	7.68	AIRS	294	4.168
HIRS 3/4	13	4.57	AIRS	108	13.831	AIRS	185	7.677	AIRS	295	4.167
HIRS 3/4	14	4.52	AIRS	111	13.796	AIRS	190	7.513	AIRS	296	4.165
HIRS 3/4	15	4.47	AIRS	112	13.768	AIRS	195	7.428	AIRS	297	4.163
HIRS 3/4	16	4.45	AIRS	113	13.739	AIRS	236	4.584	AIRS	298	4.155
HIRS 3/4	17	4.13	AIRS	114	13.621	AIRS	240	4.576	AIRS	299	4.145
HIRS 3/4	18	4	AIRS	115	13.598	AIRS	241	4.571	AIRS	300	4.133
HIRS 3/4	19	3.76	AIRS	116	13.593	AIRS	242	4.569	AIRS	301	4.088
			AIRS	117	13.564	AIRS	244	4.563	AIRS	302	4.081
			AIRS	118	13.547	AIRS	245	4.561	AIRS	303	4.074
			AIRS	119	13.541	AIRS	246	4.554	AIRS	304	4.055
			AIRS	120	13.536	AIRS	247	4.552	AIRS	305	4.013
			AIRS	125	13.376	AIRS	250	4.523	AIRS	307	3.979
			AIRS	126	13.279	AIRS	251	4.516	AIRS	308	3.949
			AIRS	127	13.239	AIRS	252	4.497	AIRS	309	3.936
			AIRS	128	13.165	AIRS	255	4.478	AIRS	311	3.845
			AIRS	134	11.85	AIRS	256	4.474	AIRS	313	3.835
			AIRS	136	10.901	AIRS	287	4.18	AIRS	314	3.83
			AIRS	137	10.884	AIRS	288	4.179	AIRS	316	3.813
			AIRS	138	10.662	AIRS	289	4.177	AIRS	318	3.791
			AIRS	179	8.087	AIRS	290	4.175	AIRS	319	3.788
									AIRS	321	3.775

The candidate IR temperature channels (Table 6) can be characterized by three main spectral groups: the longwave IR channels between 11-14 microns, a small set of water vapor channels near 7-8 microns, and a third group of shortwave IR channels spanning the 3.7-4.5 micron range. The inclusion of the water vapor channels in this section is for completeness with respect to the procedures outlined in Table 3. Using water vapor channels to interrogate the vertical temperature structure in the lower troposphere would not be ideal, due to the highly variable nature of water vapor in the atmosphere. The well-mixed gases (e.g., CO_2 and O_2) are more suitable for obtaining temperature information. Therefore, those bands with known absorption characteristics to these gases would be ideal for actual temperature structure detection.

F. EMISSIVITY PERTURBATIONS

Another factor considered in this evaluation of the sensitivity of the satellite brightness temperatures is the variability in the emissivity values in the region of the AEJ. In the simulations performed thus far, the simulations have used the default emissivity values determined by the CRTM. In this section, changes in the land surface type will be considered.   Between 8 N and 19 N along approximately 2.3 E (the longitude of the flight paths flown during the JET2000 experiment), the land surface type changes from deciduous woodlands and croplands in the south, to sparse grasslands, and finally to sandy desert farther north (Mayaux et al. 2003).

The emissivity in the passive microwave region varies with frequency and incidence angle, but is additionally affected by changes in channel polarization, vegetation cover, soil moisture, surface roughness, and the presence of standing water or snow (Prigent et al. 2006). The CRTM has a default emissivity estimate for each of the satellite sensor channels, and all calculations assume a uniform land surface. For the infrared wavelengths, the variability in the surface emissivity depends primarily on the incidence angle, frequency, and the mineralogy of the surface. To simulate the likely uncertainty in the emissivity values, the emissivity was perturbed by 3% above and below the value prescribed by the CRTM model for the MW channels and by 1% for the IR channel simulations.   These perturbations are intended to replicate actual changes in surface emissivity values through expected seasonal variability in land cover (B. Ruston, personal communication). The results of these emissivity perturbations were used as an additional test to isolate those channels that had the most sensitivity to temperature and moisture gradients in the AEJ region.

Eliminations of channels via the emissivity test in this section are then step 4 from Table 3. Selections in the channel list were based on a threshold of 1K for the emissivity evaluations. If a channel had a significant Tb signal (above 1 K) in the above moisture and temperature tests, and if the variability due to changes in the emissivity did not reduce these below 1K for either day, then that channel was considered to be best suited to remotely sense the temperature and

moisture gradients in the region controlling the location and intensity of the AEJ. The results of this test will yield the best channels for obtaining remotely-sensed data regarding the moisture and temperature gradients when emissivity perturbations are applied.

1. Moisture Candidate Channels

Of the 11 MW moisture candidate channels in table 5, only the AMSU-B channel 5 (183.3+/-7 GHz) and MHS channel 5 (190.3 GHz) provided moisture gradient information above a 1 K Tb difference when emissivity perturbations of +/-3% are applied. The comparable channel on the SSMI/S instrument (channel 9,183.31+/-6.6 GHz) did not meet the 1 K threshold for each day when emissivity perturbations were applied. Presumably this difference in sensitivity is due to the longer path length taken by photons that are received by the conical-scanning SSMI/S instrument. To evaluate the effect this scanning angle would have on AMSU-B channel 5, the CRTM was programmed to simulate the Tb output for the Case 2 results at a 53.1 degrees satellite inclination angle. At this simulated inclination angle, AMSU-B channel 5 had slightly more sensitivity (approximately 0.2 K) than the SSMI/S simulation for channel 9. Another sensitivity test was performed to see at what angle the AMSU-B channel 5 would fall below the 1 K Tb difference threshold. This test determined that at approximately 30 degrees from nadir, the threshold value was no longer met.

The 21 IR candidate channels in Table 5 were evaluated to assess the impact of 1% emissivity perturbations on the simulated Tb differences. This evaluation indicated that only one channel, the AIRS 13.165 micron, was eliminated due to changing the emissivity values by 1%. This elimination was due to the relatively weak 1.20 K Tb difference exhibited for the 28 August simulation of the lower-tropospheric moisture gradient. When uncertainty due to emissivity perturbations is applied, a value of +/- 0.30 K was determined for this channel, which reduced the simulated signal below the desired 1 K threshold. A final list of the channels that indicated moisture sensitivity while accounting for emissivity perturbations is included in Table 7.

Table 7.   Candidate channels as in Table 5, except also being robust to emissivity perturbations for detecting moisture gradients below the 650 mb level. AIRS channel numbers refer to the 324 channel subset.

Microwave Instruments			Infrared Instruments		
Instrument	Ch #	Channel	Instrument	Ch #	Channel
AMSU-B	5	183.3+/-7	HIRS 3/4	7	13.35
MHS	5	190.3	HIRS 3/4	19	3.76
			AIRS	108	13.831
			AIRS	111	13.796
			AIRS	112	13.768
			AIRS	113	13.739
			AIRS	125	13.376
			AIRS	126	13.279
			AIRS	127	13.239
			AIRS	179	8.087
			AIRS	181	7.991
			AIRS	182	7.779
			AIRS	183	7.742
			AIRS	190	7.513
			AIRS	313	3.835
			AIRS	316	3.813
			AIRS	318	3.791
			AIRS	321	3.775

2.   Temperature Candidate Channels

The candidate list for MW channels considered sensitive to temperature perturbations below 650 mb was not changed when +/-3% perturbations to the surface emissivity were taken into account. The largest magnitude emissivity perturbations were noted for channels in the 89-91 GHz range, but this change was only on the order of 0.49-0.53 K Tb difference. Since each of these channels had Tb difference values of at least 7.5 K, the emissivity uncertainty was not considered significant for these channels. Thus, the MW channels in Table 5 are considered to be the best channels for interrogating the temperature gradients responsible for the AEJ location and intensity.

The results for the IR emissivity sensitivity tests were the same, since none of the channels in Table 6 fell below the desired Tb difference threshold of 1 K for the temperature simulations. Thus, the channels in Table 6 represent those IR channels that can best provide information about the temperature gradient that controls the AEJ.

G.   OBSERVED GRADIENT SENSITIVITY: CASE 3

In the previous sections, the Tb outputs were for the moisture and temperature simulated profiles in Cases 1 and 2 that were a blend of in-situ data and model data that were modified above 650 mb. In this third case, the complete vertical SAL and non-SAL profiles were inserted in the CRTM with realistic land cover information and emissivity perturbations for the northern (SAL) and southern (non-SAL) points, respectively. The results from the observed cases were evaluated to answer the following questions: Is there an observed Tb gradient between the SAL and non-SAL air masses for the selected 28 August and 29 August observed profiles? What can be said of the nature of the observed Tb gradient with respect to the simulation Cases 1 and 2?

The Tb gradients from the CRTM with realistic conditions were examined for each day to evaluate which channels did exhibit a Tb gradient above the 1 K Tb difference threshold. Channels selected based on the results from Cases 1 and 2 will be used to interpret the contributions for the channels that meet the sensitivity criterion.

Each of the simulated profile candidates for the moisture gradients presented in Table 7 demonstrated Tb gradient values well in excess of the 1 K threshold. However, the contributions to resolving this Tb gradient cannot be separated explicitly as being due to temperature or moisture individually. In all of the MW channels analyzed, the channels that had sensitivity to emissivity perturbations also had a much larger Tb difference, so that uncertainty due to emissivity did not reduce any of the results below the 1 K threshold. Likewise, the temperature sensitive channels selected through the evaluations performed in Case 2 and presented in Table 6 also had a large Tb gradient in the observed case with no channels reduced below 1 K due to emissivity perturbations.

It should be noted that moisture and temperature variations do not have the same effect on the Tb output. For example, increases in temperature yield an increase in brightness temperature for all frequencies. However, increases in water vapor do not always cause an increase in Tb. For the IR channels, this

increase in water vapor results in a decrease in Tb. In the MW channels, an increase in Tb can occur depending on the surface emissivity value and sea-surface temperature of an ocean surface, an increase in water vapor can actually appear warmer due to the relatively lower emissivity value of the ocean surface. In this case, the atmospheric contribution provides a larger Tb signal than the surface. The opposite may be true over land, since the emissivity values over land are much higher than ocean surfaces. An increased emissivity value over land will thus yield a lower Tb value for an increase in atmospheric water vapor.

The largest MW Tb gradient in the observed Case 3 was from the AMSU-B channel 5 (183.3+/-7 GHz) on 28 August, and by MHS channel 3 (183.3+/-1 GHz) on 29 August. These results agree with the Tb differences from the simulated lower-tropospheric moisture structure in Case 1 between 28 August and 29 August (Figures 12 and 13, respectively). On 28 August, the difference in moisture between the SAL and non-SAL air mass was greater than the 29 August SAL and non-SAL moisture difference. AMSU-B channel 5 has peak sensitivity to water vapor lower in the atmosphere than MHS channel 3. For the IR channels, the largest gradient was from the AIRS 7.598 and 6.361 micron channels for 28 August and 29 August, respectively.

For the MW instruments evaluated, all of the channels evaluated using the 28 August complete T and q observed profiles indicated sensitivity above the 1 K Tb threshold, with the exception of the channels in the 54-55 GHz band. The results for the 54-55 GHz channels are consistent with the results found in the Case 1 and Case 2 simulations. These frequencies lie in the O2 absorption band, and likely peak at a high altitude.

For the 28 August Tb differences, the IR channels near 14 microns did not have a significant sensitivity. This region of the IR spectrum is a CO_2 absorption band that is ideal for obtaining atmospheric vertical temperature information. The 14-14.2 micron channels on the AIRS instrument did indicate sensitivity above the 1 K threshold for the 29 August profiles, but these responses are most likely

due to the changes in temperature gradients in the upper troposphere, where the 29 August temperature gradient is stronger than the 28 August temperature gradient.

H.   CASE STUDY 22-23 JULY 2006

In the above tests, the CRTM has been used to simulate the Tb output to determine which channels are the most sensitive to the features that control the location and intensity of the AEJ. In this section, satellite imagery during the African Multidisciplinary Monsoon Activity (AMMA) will be examined to illustrate which of the candidate channels for moisture and temperature provides the best signature of the differences between the SAL and non-SAL air masses.

The case selected was suggested by Jason Dunion of the NOAA Atlantic Oceanographic and Meteorological Laboratory, Hurricane Research Division, who had detected a significant SAL outbreak on 22-23 July 2006. This case will be used to examine the contrast between the SAL air mass to the north and the non-SAL air mass to the south of the AEJ. A brief description of the synoptic situation will be provided to facilitate the discussion of a select set of satellite images.

1.   Synoptic Situation 22-23 July 2006

On 22 July 2006, the AEJ was located at approximately 13 N, and extended east-west between 10 E and 30 W. A high pressure ridge was over the western North Atlantic just off the northwestern coast of Africa. To the south of the AEJ, moist air was associated with onshore flow across the southern coastal region of the West African continent. The monsoon trough was well established over northern Mali, and extended westward over central Mauritania toward the coastline. The Global Forecasting System (GFS) model analyses for Africa are included in Figure 30. An MCS moving east to west can be identified in the Meteosat-8 image (Figure 31) near the latitude of the AEJ. The cloud-contaminated nature of the area to the south of the AEJ is evident in the image, while the SAL air mass to the north of the AEJ is largely cloud-free.
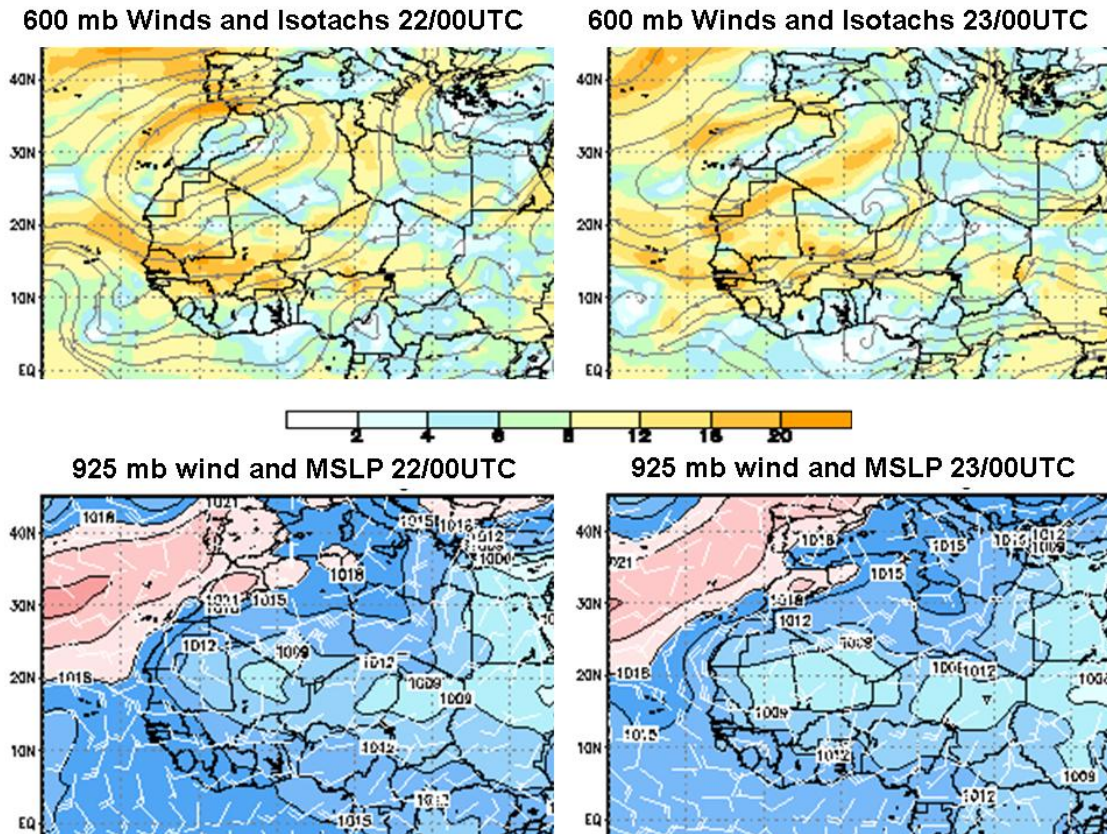
Figure 30.   (top) GFS 600 mb streamlines and isotachs (see scale) for 00 UTC 22 July 2006 (left) and 00 UTC 23 July 2006 (right). (bottom) Corresponding mean sea-level pressure analyses associated with the West African monsoon trough that extends to the coast on the 23rd. In the upper charts, the 600 mb depiction of the AEJ can be identified near 13 N as a band of 18-20 m/s winds over continental Africa. [Images cropped from those available at http://aoc.amma-international.org/nwp/globalmodel/ncep/ncep-gfs/].

One advantage of using the 22-23 July 2006 case as a comparison with the simulated tests in Cases 1 and 2 earlier is that an MCS moves through the region of interest in a similar way as an MCS moved through the AEJ region during the JET2000 experiment.   This situation allows for a comparative evaluation of the day-to-day observed satellite imagery Tb gradients and any changes that may occur.
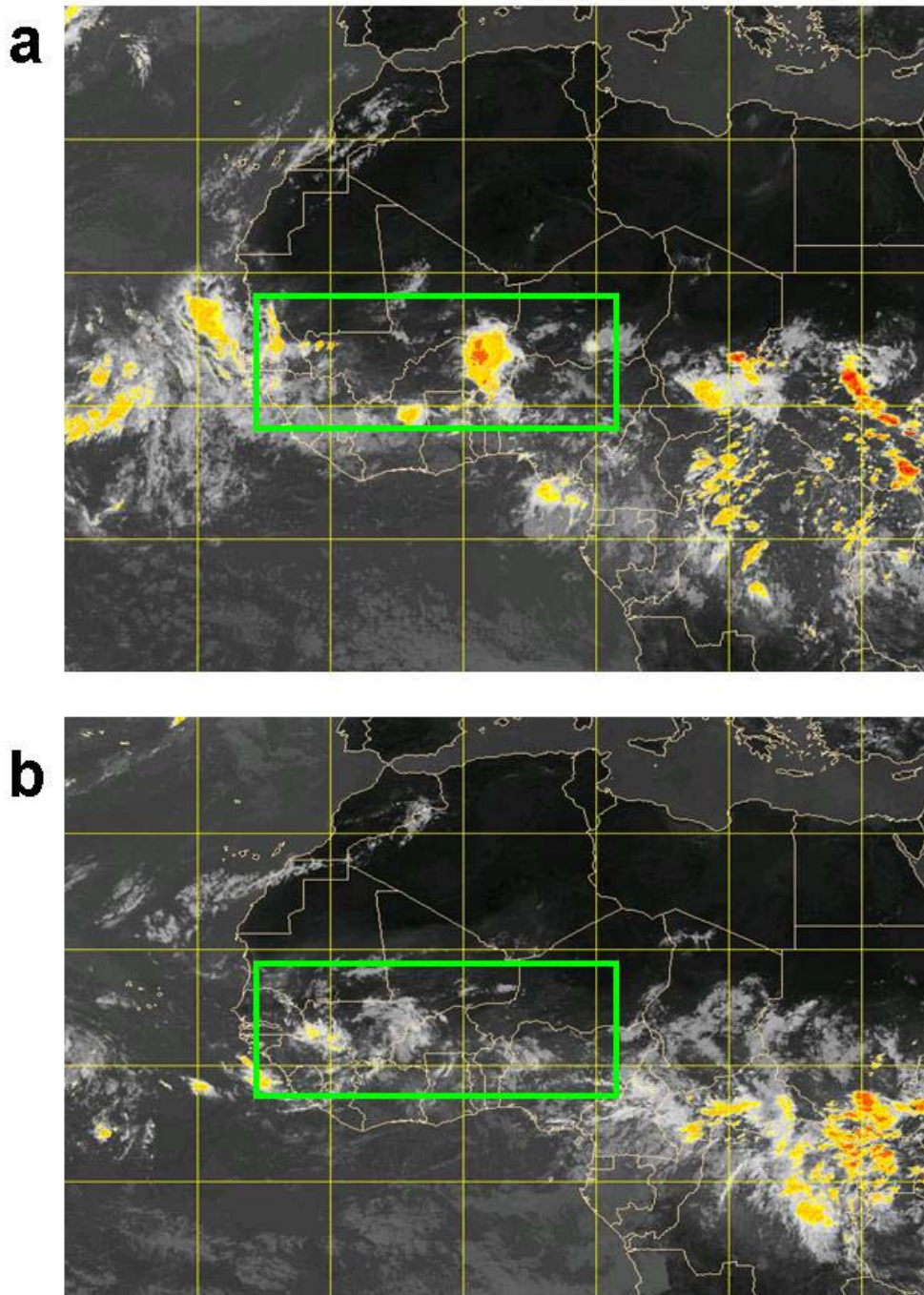
Figure 31.   Enhanced IR image from Meteosat 8 at 1200 UTC (a) 22 July 2006 and (b) 23 July 2006 over western Africa. Green boxes delineate the area of interest with respect to gradient evaluations for each day [From http://aoc.amma-international.org/observation/satellite].

2. Moisture Channels

a. *AMSU-B 183.3+/-7 GHz*

Based on the results from Case 1, the best MW channels to detect the moisture gradient over the AEJ region are the AMSU-B 183.3+/-7 GHz and the MHS 190.3 GHz channel. Both of these channels detected changes in the moisture structure below 650 mb even when expected emissivity perturbations were applied. The ascending AMSU-B channel 5 image for 22 July (Figure 32) illustrates the sharp gradient between the SAL and non-SAL air masses. The best possible Tb gradient estimates will be concentrated near the scan-center regions. The cloud-free regions within the box indicate a Tb gradient of approximately 15 K, which is well above the value for this channel in the Case 1 simulations, but very close to the value from Case 3.

NOAA-17 AMSU-B CH 5 183.3+/-7 GHz 20060722 1806 to 0046 UTC

Figure 32. AMSU-B channel 5 (183.3+/-7 GHz) image from 22 July 2006. Black boxes indicate region of interest with respect to the moisture gradient (Image provided by Nancy Baker, NRL).
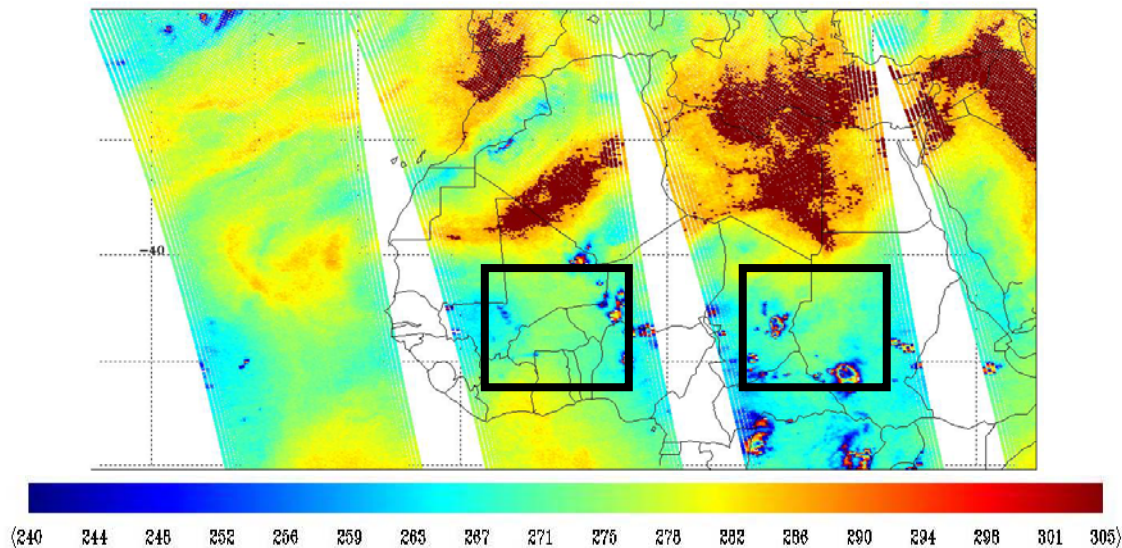
Figure 33.   As in Figure 32, except for 23 July 2006 (Image provided by Nancy Baker, NRL).
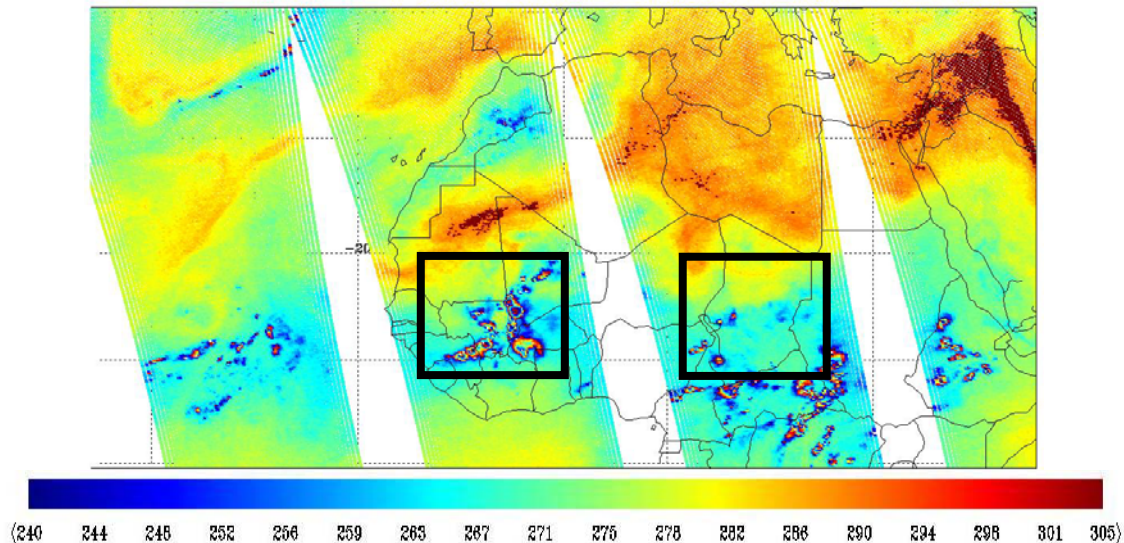
After the MCS moves through the region, the lower-tropospheric moisture gradient has been modified through convective processes due presumably to downdraft activity and convective transport of moisture. Within 24 hours, the lower-tropospheric moisture gradient has become somewhat obscured, but it is still evident due to the approximately 5 K Tb gradient within the regions marked in Figure 33. This change in Tb gradient is analogous to the changes in Cases 1 and 3, where it was due to the changes in vertical moisture structure observed during the JET2000 experiment.

b.   AIRS 7.513 Micron

The AIRS 7.513 micron channel demonstrated the best IR response to the lower-tropospheric moisture perturbations in Case 1. The Tb gradient in the 7.513 image for 22 July 2006 (Figure 34) is comparable to that of the AMSU-B image in Figure 30 with a magnitude near 15 K. Increased moisture absorption along the path toward the edge of scan results in Tb values that are sensed at higher (and thus cooler) levels in the atmosphere relative to the center of scan. If a forecaster wanted to qualitatively locate the lower tropospheric moisture gradients associated with the AEJ, both the AMSU-B 183.3+/-7 GHz

and the AIRS 7.513 micron channels would provide the most relevant information. However, qualitatively resolving the actual moisture gradient is a much more complicated process involving knowledge of the channel's temperature and moisture sensitivity, the channel's signal to noise ratio, and the contributions due to the surface emission. The AIRS 7.513 micron channel is subject to absorption due to CO_2, but this effect is not as large as the amount of water vapor absorption for this channel, as indicated by the gaseous atmospheric transmittance values for water vapor and CO_2 from Figure 4. Corresponding AIRS imagery was not available for the 23 July case, but the 22 July image is included here to illustrate the capability of this IR candidate channel.
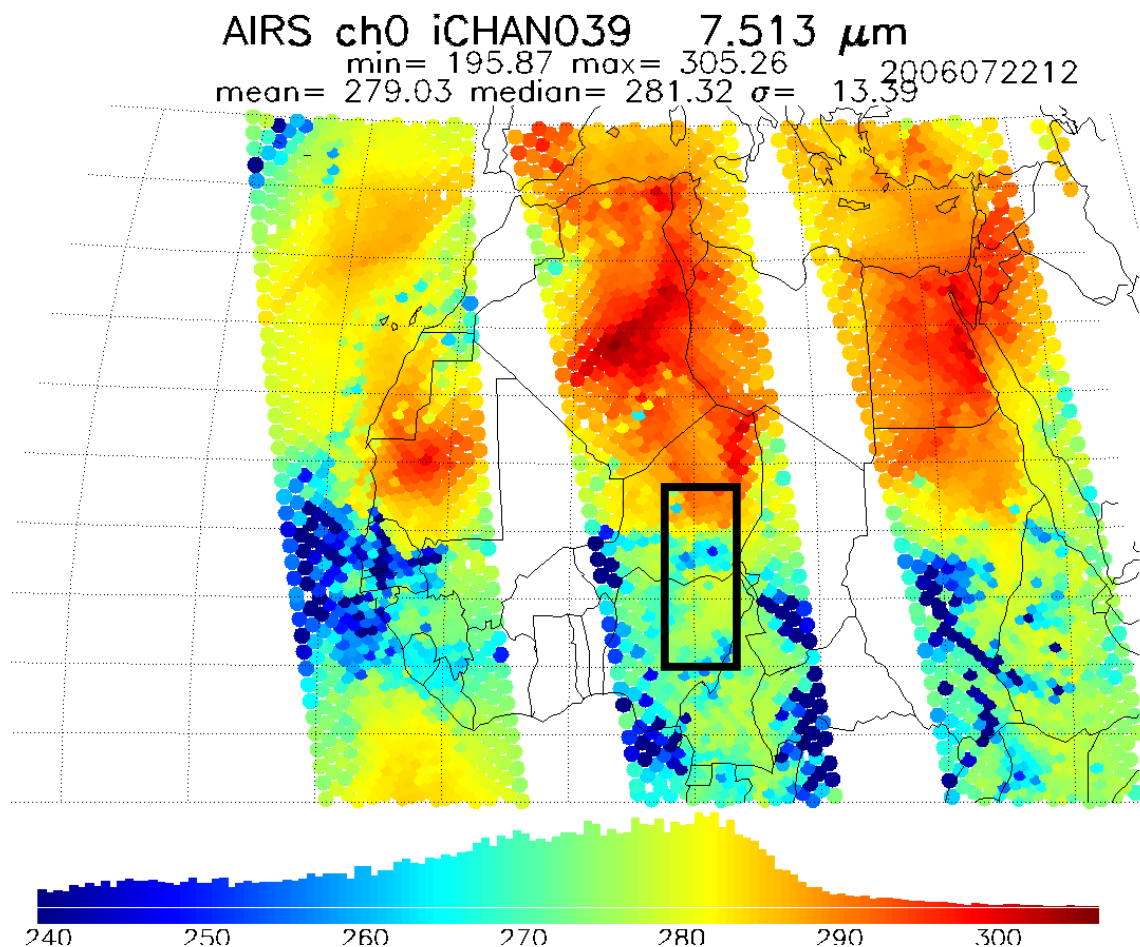
Figure 34.   AIRS 7.513 micron channel image from 22 July 2006. Black box indicates area of interest with respect to the gradients evaluated in this study (Image provided by Ben Ruston NRL).

3. Temperature Channels

The analysis of Case 2 revealed several candidate channels (35 MW and 95 IR) that would provide the desired sensitivity to temperature gradient perturbations below 650 mb, and were not degraded by expected changes in emissivity values over the region of interest. Some of the channels exhibiting the largest responses will be examined using satellite imagery. Only a few examples from the SSMI/S and AIRS instruments will be presented as representative for conical-scanning MW instruments and cross-track scanning IR instruments, respectively.

a. SSMI/S 19.35 GHz V

The SSMI/S channel most sensitive to the temperature perturbations in Case 2 is the 19.35 GHz V channel 13. The SSMI/S channel 13 image from 1000 UTC on 22 July 2006 (Figure 35) clearly distinguishes between the cooler air to the south of the AEJ and the hot Saharan air to the north. The Tb values between the northern and southern air masses on the image range from 275-290 K within the area of interest. Since the conical-scanning SSMI/S maintains a near-constant look angle relative to the Earth surface, the Tb gradient can be estimated across the full scan width.
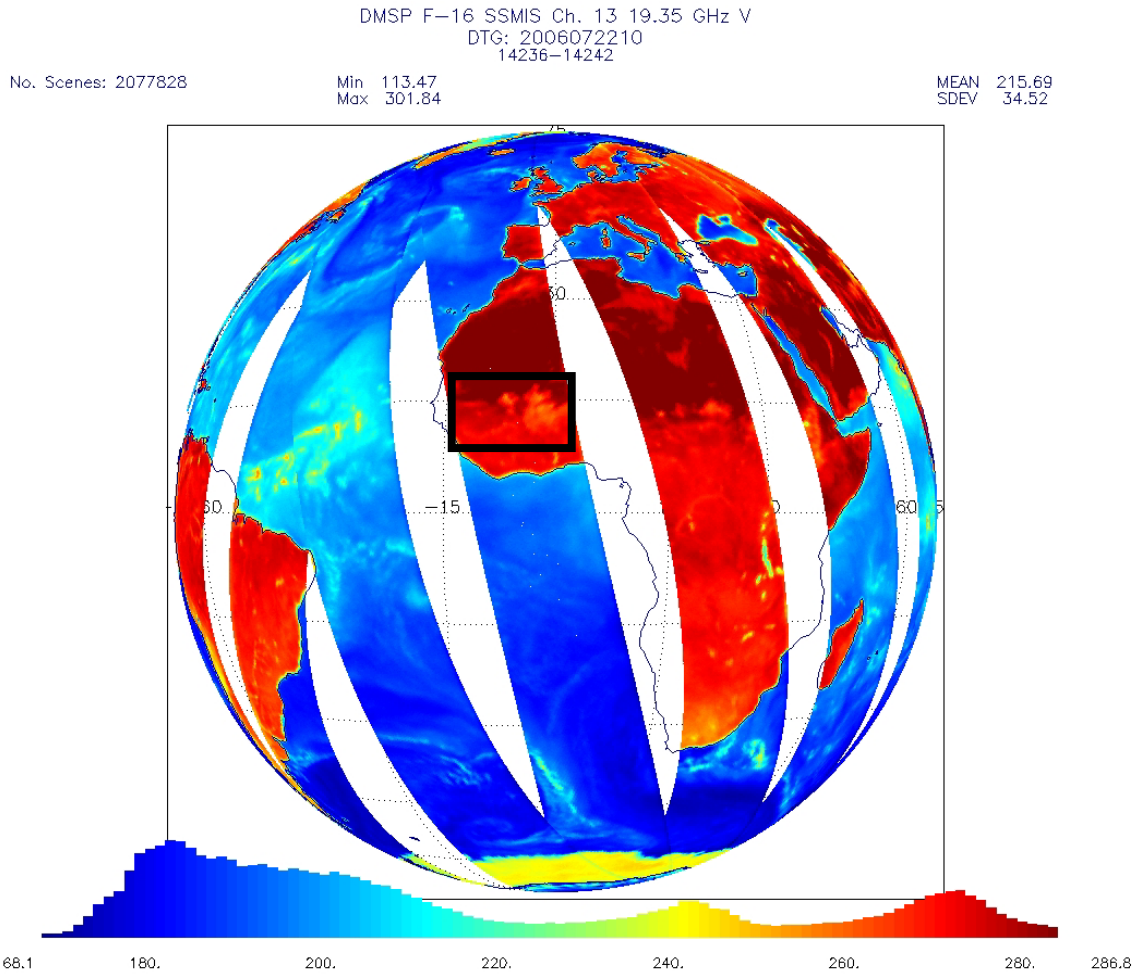
Figure 35.   SSMI/S channel 13 image from 1000 UTC 22 July 2006. Black box outlines the area of interest with respect to interrogating the lower-tropospheric temperature gradient (Image provided by Steve Swadley, METOC Consulting)
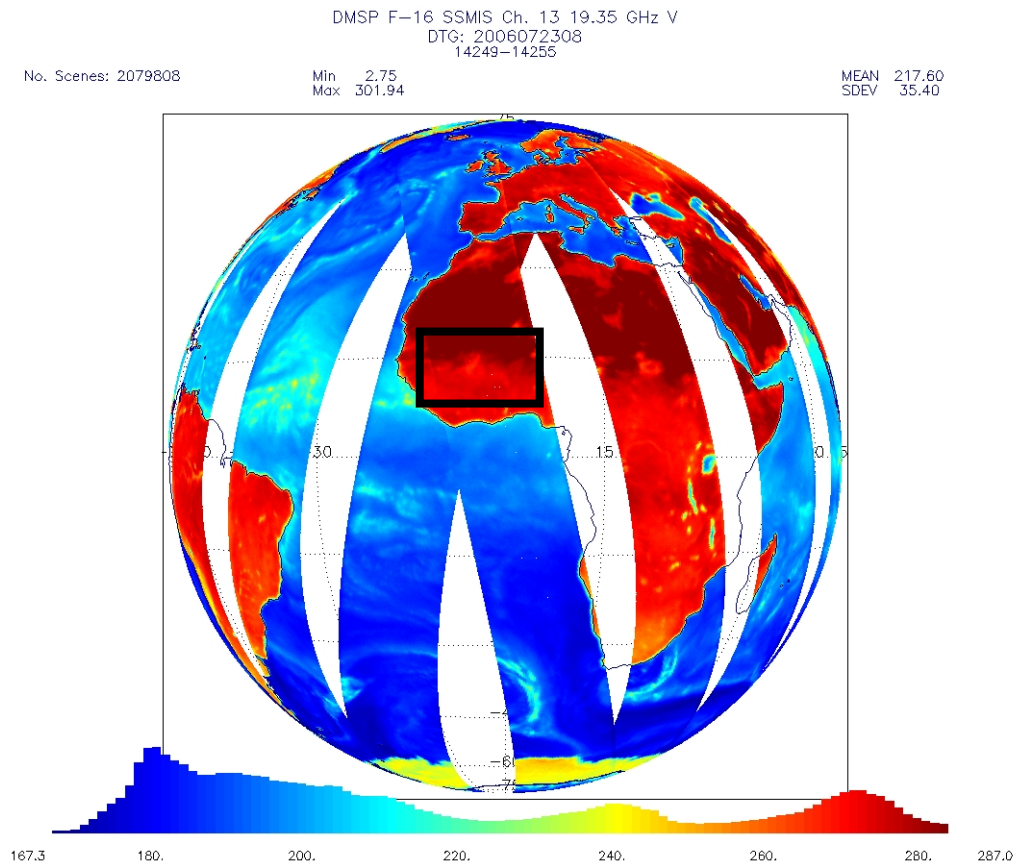
Figure 36.   As in Figure 35, except for 23 July 2006 (Image provided by Steve Swadley, METOC Consulting).

The Tb gradient observed on 23 July 2006 (Figure 36) over the same region is approximately 5 K weaker than that observed on 22 July. However, the similarities between the pattern and location of the temperature gradient between these two days is very similar, and is an example of the smaller cloud water vapor impacts in the lower frequency MW bands.

b.   AIRS 10.622 Micron

The AIRS 10.622 micron channel had the largest response to the temperature perturbations in Case 2. In the AIRS 10.662 channel (Figure 37), the observed Tb values range from 295-315 K between the non-SAL and SAL regions, respectively. The cooler pixels in the center of scan are presumed to cloud-contaminated. Although the actual temperature gradient for the 22 July case is unknown for the region analyzed, these values appear to be reasonable

compared to Case 3 Tb values based on the CRTM output using the JET2000 observations over the SAL and non-SAL regions.

Figure 37.   AIRS 10.662 micron channel for 12 UTC 22 July 2006.   Black box identifies the center of scan area of interest with respect to the temperature gradient estimation (Image provided by Ben Ruston, NRL).

THIS PAGE INTENTIONALLY LEFT BLANK

IV.   CONCLUSIONS AND FUTURE WORK

The CRTM has been used to determine which channels are best suited to obtain polar-orbiting remotely-sensed observations o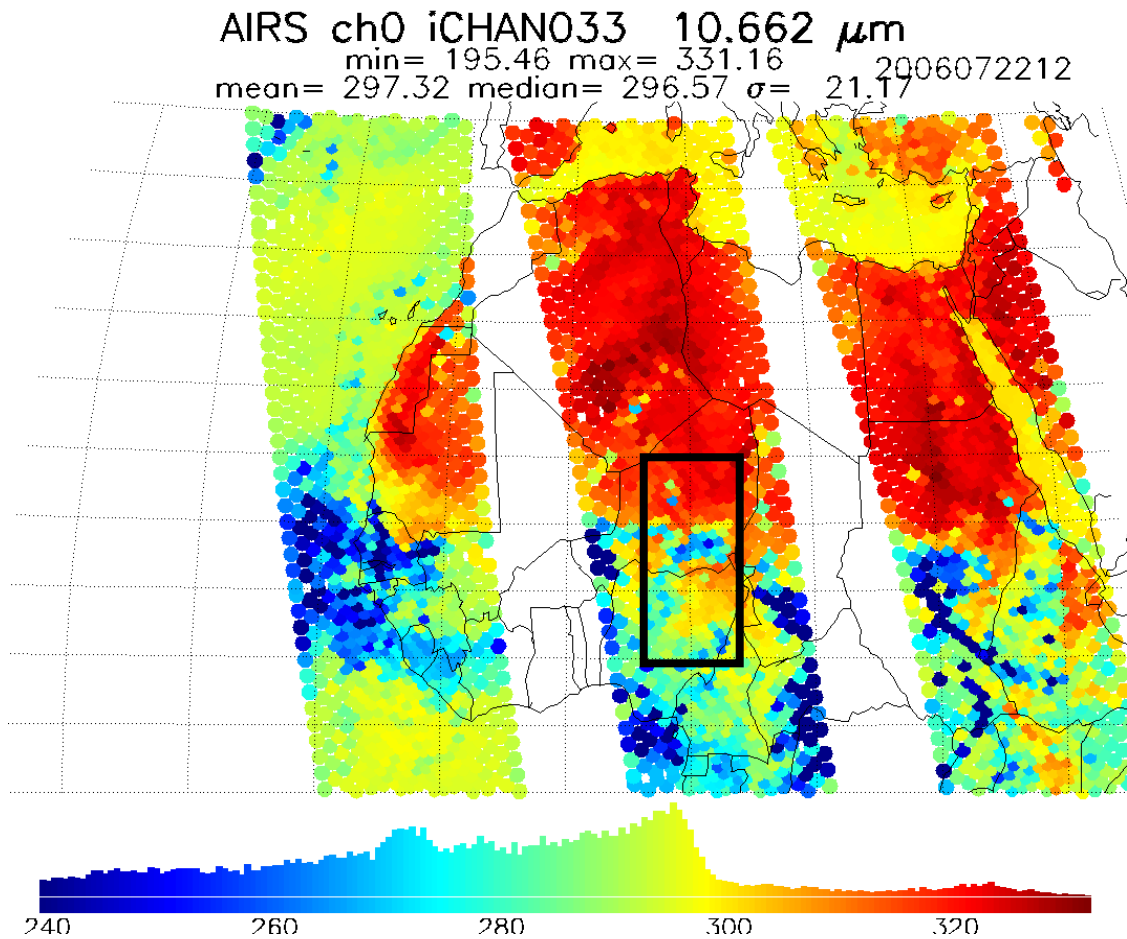f the lower-tropospheric moisture and temperature gradients related to the location and intensity of the AEJ over continental West Africa. Temperature and moisture profiles derived from dropsonde reports from the northern (SAL) and southern (non-SAL) ends of the JET2000 flights on 28 and 29 August 2000 were blended with ECMWF analyses and used to provide the input parameters for the CRTM. These blended profiles were then used to create simulations to isolate the moisture (temperature) signal output from the CRTM. For the simulated examples presented in Case 1 and Case 2, the average of the northern and southern profiles provided the input temperature and moisture above 650 mb. In order to separately address the moisture (temperature) signature, the average of the northern and southern temperature (moisture) profiles was combined with the respective observed moisture (temperature) profile values below 650 mb to provide the input for Case 1 (Case 2). In Case 3, the full moisture and temperature profiles were input to the CRTM on both days. In each case, expected changes to surface emissivity values were applied. Any instrument channel response that did not meet a brightness temperature (Tb) threshold of 1 K was eliminated from further consideration.

A.   MOISTURE GRADIENT ESTIMATION

1.   Microwave Instruments

Based on the simulations performed in Case 1, the best channels to evaluate the moisture gradient below 650 mb are summarized in Table 4, which includes 11 candidate MW channels from the SSMI/S, AMSR-E, AMSU-B, and MHS instruments. These channels had the largest response to the lower-tropospheric moisture gradient on both days. A final step in Case 1 was the inclusion of surface emissivity perturbations that would be expected to occur due to changes in land surface type over the AEJ region. After applying the

emissivity perturbations of +/-3%, the candidate MW channel list is reduced to only two channels, the AMSU-B 183.3+/-7 GHz and the MHS 190.3 GHz channel.

In Case 3 with the full northern and southern JET2000 profiles, the selected MW channels did have Tb difference values exceeding 1 K using realistic emissivity values and perturbations. However, it is not clear to what extent the north-south temperature gradient contributed to the Tb response in the two selected MW channels. Since contributions to the Tb values can come from both temperature and moisture structures, the source of the Tb gradient was examined using satellite imagery for the AMSU-B 183.3+/-7 GHz channel over the AEJ region during a SAL outbreak on 22-23 July 2006. A marked Tb gradient does exist, with a larger magnitude Tb difference than in the Case 1 results. Thus, the Tb difference between the Cases 1 and 3 may indicate that the differences in the day-to-day average temperature profiles used in Case 1 may also contribute to the difference in the Tb signal. The process of resolving the lower-tropospheric moisture gradient from Tb values cannot be correctly accomplished without simultaneously considering the contribution due to changes in surface emission and temperature, which for the latter may change more rapidly than the moisture gradient.

2.   Infrared Instruments

The infrared instruments examined in this study include the HIRS 3 and 4 as well as the AIRS. An important caveat for the IR test is the assumption that the region is not cloud-contaminated. By isolating the moisture gradient below 650 mb in Case 1, a total of 21 IR channels from the AIRS, HIRS 3, and HIRS 4 instruments were appropriate for evaluating the moisture gradient (Table 4). The most sensitive channels were in three spectral regions of the IR: 3.76-3.8 microns, 7.5-8 microns, and 13.1-13.3 microns. Note that for the 3.76-3.8 micron channels the CRTM assumes a constant solar zenith angle of 45 degrees. Actual use of these channels for interrogation of the moisture gradient over this area would have to account for changes in Tb received based on contamination due to reflected solar radiation. For the 7.5-8 micron and the 13.2-13.3 micron

channels, the CRTM assumes the amount of CO_2 in the atmosphere as fixed, however variability in CO_2 content is expected to have a minimal effect due to the well-mixed nature of CO_2 in the atmosphere. Allowing for a +/-1% IR emissivity over the source region of the AEJ resulted in the reduction of the list in Table 4 to a total of 20 candidate IR channels.

B. TEMPERATURE GRADIENT ESTIMATION

1. Microwave Instruments

In case 2, an average moisture profile was used with the observed temperature profiles below 650 mb to evaluate the response of the MW channels to the north-south temperature differences across the Sahel. A total of 35 MW channels (Table 5) were found to have significant Tb response, 24 channels more than were identified with Case 1 for the moisture gradient. The MW channels with the most sensitivity to the north-south temperature differences in Case 2 were in the window regions of the MW spectrum and in the ranges 6-37 GHz, 89-91.655 GHz, and 150 GHz. Of these 35, no channels were removed due to +/-3% changes in emissivity values. Each MW candidate channel exhibited a strong simulated Tb gradient compared to the magnitude of the Tb uncertainty due to the emissivity changes.

2. Infrared Instruments

The Case 2 tests revealed 95 candidate IR channels from the AIRS and HIRS 3/4 instruments as suitable for detecting the temperature gradient responsible for the location and intensity of the AEJ (Table 6). The IR channels best suited for evaluating the temperature gradient are in the following spectral ranges: 3.76-4.5 microns, 7.4-8 microns, 10.6-11 microns, and 13-14 microns. Among these channel groupings, the effects due to CO_2 were not analyzed since it is assumed to be well mixed, fixed gas in the CRTM. The 13-14 micron channels are also impacted by absorption due to O_3 (not considered in this study), but based on the transmittance diagram (Figure 4), this impact is expected to be minimal. Similar to the MW channel results from Case 2, none of the IR channels lost the desired amount of sensitivity due to +/-1% emissivity perturbations.

C.   FUTURE WORK

Using the CRTM to simulate Tb output provides a unique capability to evaluate which types of satellite sensors and channels should be most effective to observe the lower-tropospheric moisture and temperature gradients in the AEJ region. The use of the CRTM allowed for evaluation of sensors that were not in orbit at the time of the JET2000 experiment. In this study, both types of satellite instruments (conical- and cross-track scanning) and various frequencies or wavelengths were found to be appropriate for gaining information related to the AEJ location and intensity. The CRTM could also be used to model the Tb output for proposed new sensors and for validation over areas of particular interest, before these sensors are placed in orbit. Studies of this nature could impact decisions about the frequencies used and types of satellites (conical- versus cross-track scanning) to design and use in the future.

One limitation of this study is that only two days of JET2000 observations sampled the north-south changes in atmospheric structure in the region of the AEJ. Thus, recent observations collected during the on-going AMMA experiments could be evaluated as they become available for a more complete and comprehensive study of contemporary and future satellite systems. Use of AMMA data could allow for a direct comparison between CRTM simulated Tb values and those observed by operational satellite instruments.

One of the key properties of the different MW and IR instrument channels is the horizontal resolution provided by each channel. For the IR this variability is dependant on sensor, i.e., the aperture size determines the resolution of the sensor. As MW frequency decreases, the satellite antenna size must increase to maintain a constant field of view. This can become impractical when considering costs (and weight) associated with placing high resolution/low frequency MW instruments in orbit. Future studies could examine what effect these differences in horizontal resolution have on the detection of the lower-tropospheric temperature and moisture gradients in the region between the SAL and non-SAL air masses. Since the baroclinic (temperature gradient) zone and moisture gradient slope upward toward the equator, the satellite instruments need to also

resolve the vertical gradients in this region. By using the JET2000 (or AMMA) data as input, the CRTM output could readily be modified to examine both horizontal and vertical resolution effects.

One of the advantages of using remotely-sensed data is the large amount of data gathered over relatively short periods of time. Based on the results of this work, a variational assimilation of selected channel brightness temperatures could be performed to evaluate the impact of subsequent model forecasts. Various data-denial studies could also be performed to further refine the list of best channels/sensors for measuring parameters over the AEJ source region.

The JCSDA is constantly working to improve the capabilities of the CRTM with respect to gaseous absorption and the impact of aerosols on Tb simulations. One of the prominent features of the SAL (not examined here) is the large amount of dust aerosol scoured from the surface by convectively driven downbursts.   When the CRTM can compute equivalent dust contaminated brightness temperature values, the impact of this dust aerosol in the SAL should be an important objective in future satellite remote sensing studies of the formation and maintenance of the AEJ.

THIS PAGE INTENTIONALLY LEFT BLANK

LIST OF REFERENCES

Burpee, R. W., 1972: The origin and structure of easterly waves in the lower troposphere of North Africa. *J. Atmos. Sci.,* **29**, 77-90.

Carlson, T. N., and J. M. Prospero, 1972: The large-scale movement of Saharan air outbreaks over the northern equatorial Atlantic. *J. Appl. Meteor.,* **11,** 283–297.

Charney, J. G., and M. E. Stern, 1962: On the stability of internal baroclinic jets in a rotating atmosphere. *J. Atmos. Sci.*, **19**, 159-172.

Dunion, J. P., and C. S. Velden. 2004: The impact of the Saharan air layer on Atlantic tropical cyclone activity. *Bull. Amer. Meteor. Soc.,* **85**, 353–365.

English, S. J., 2004: Assessment of the requirement for 23.6-24.0 GHz observations for weather forecasting. Tech. Rep. 440, 6 pp. [Available from National Meteorological Library, Fitzroy Road, Exeter, UK.]

Karyampudi, V. M., and T. N. Carlson, 1988: Analysis and numerical simulations of the Saharan air layer and its effect on easterly wave disturbances. *J. Atmos. Sci.,* **45,** 3102–3136.

Karyampudi, V. M., and H. F. Pierce, 2002: Synoptic-scale influence of the Saharan air layer on tropical cyclogenesis over the eastern Atlantic. *Mon. Wea. Rev.,* **130**, 3100–3128.

Landsea, C.W., 1993: A climatology of intense (or major) Atlantic hurricanes. *Mon. Wea. Rev.*, **121**, 1703-1713.

LeMarshall, J.L., F. Weng, S. Lord, L.P. Riishojgaard, P. Phoebus, and J. Yoe, 2005: Recent advances at the Joint Center for Satellite Data Assimilation. Paper 2.1, *Extended Abstracts. Ninth Symposium on Integrated Observing and Assimilation Systems for the Atmosphere, Oceans, and Land Surface,* Amer. Meteor. Soc., 2.1. San Diego, CA

Mayaux P., E. Bartholomé, M. Massart, C. Van Cutsem, A. Cabral, A. Nonguierma, O. Diallo, C. Pretorius, M. Thompson, M. Cherlet, J-F. Pekel, P. Defourny, M. Vasconcelos, A. Di Gregorio, S. Fritz, G. De Grandi , C. Elvidge, P. Vogt, A. Belward, cited 2007: The Land Cover of Africa for the Year 2000. [Available online at http://www-gvm.jrc.it/glc2000/Workshops/March2003/Presentations/Mayaux_Africa_overview.pps]

NCEP, cited 2006: Monthly Global Data Assimilation System (GDAS) input data counts. [Available online at http://www.nco.ncep.noaa.gov/sib/counts/May_2006.html]

Pardo, J.R., J.P. Encrenaz, and D. Breton, cited 2007: Utilization of the radiofrequency spectrum above 1GHz by the EES (passive) service and interference criteria. [Available online at http://damir.iem.csic.es/PARDO/uit_breton.doc]

Prigent, C., F. Aires, and W.B. Rossow, 2006: Land surface microwave emissiviites over the globe for a decade. *Bull. Amer. Meteor. Soc.,* **87,** 1573-1584.

Pytharoulis, I., and C.D. Thorncroft, 1999: The low-level structure of African easterly waves in 1995. *Mon. Wea. Rev.*, **127**, 2266-2280.

Reed, R. J., D. C. Norquist, and E. E. Recker, 1977: The structure and properties of African wave disturbances as observed during Phase III of GATE. *Mon. Wea. Rev.*, **105**, 317-333.

Thorncroft, C. D., D. J. Parker, R. R. Burton, M. Diop, J. H. Ayers, H. Barait, S. Devereau, A. Diongue, R. Dumelow, D. R. Kindred, N. M. Price, M. Saloum, C. M. Tayor, and A. M. Tompkins, 2003: The JET2000 project: Aircraft observations of the African Easterly Jet and African Easterly Waves. *Bull. Amer. Meteor. Soc.*, **84**, 337-351.

Air Force News, cited 2007: Africa command close to becoming a reality. [Available online at http://aimpoints.hq.af.mil/display.cfm?id=15734]

Weng, F., cited 2007: Joint Center for Satellite Data Assimilation Community Radiative Transfer Model (CRTM): Surface emissivity models. [Available online at http://geo.obspm.fr/workshop/S1.02.FWeng.ppt]

Whelan, T., cited 2007: Africa's ungoverned space: A new threat paradigm. [Available online at http://www.jhuapl.edu/POW/rethinking06/video.cfm]

Yong, H., P.V. Delst, Q. Lui, F. Weng, B. Yan, J. Derber, cited 2007: User's Guide to the JCSDA Community Radiative Transfer Model (Beta Version). [Available online at http://www.orbit.nesdis.noaa.gov/smcd/spb/CRTM/crtm-code/CRTM_UserGuide-beta.pdf]

INITIAL DISTRIBUTION LIST

1.   Defense Technical Information Center
      Ft. Belvoir, Virginia

2.   Dudley Knox Library
      Naval Postgraduate School
      Monterey, California

3.   Air Force Institute of Technology
      Wright-Patterson Air Force Base, Ohio

4.   Naval Research Laboratory Library
      Naval Research Laboratory
      Monterey, California

5.   R.L. Elsberry
      Naval Postgraduate School
      Monterey, California

6.   N. Baker
      Naval Research Laboratory
      Monterey, California

7.   C. Blankenship
      Naval Research Laboratory
      Monterey, California

8.   B. Ruston
      Naval Research Laboratory
      Monterey, California

9.   Z. Wang
      Naval Postgraduate School
      Monterey, California